Diverse phage defence systems define West African South American pandemic *Vibrio cholerae*

David W. Adams[1,2]*, Milena Jaskólska[1], Alexandre Lemopoulos[1], Sandrine Stutzmann[1], Laurie Righi[1], Loriane Bader[1] and Melanie Blokesch[1,2]*

[1]Laboratory of Molecular Microbiology, Global Health Institute, School of Life Sciences, Station 19, EPFL-SV-UPBLO, Ecole Polytechnique Fédérale de Lausanne (EPFL), CH-1015 Lausanne, Switzerland.

[2]These authors contributed equally.

*Corresponding authors: david.adams@epfl.ch and melanie.blokesch@epfl.ch

Summary

Our understanding of the factors underlying the evolutionary success of different lineages of pandemic *Vibrio cholerae* remains incomplete. Interestingly, two unique genetic signatures define the West African South American (WASA) lineage of *V. cholerae* responsible for the 1991-2001 Latin American cholera epidemic. Here we show these signatures encode diverse anti-phage defence systems. Firstly, the WASA-1 prophage encodes a 2-gene abortive-infection system WonAB that renders the lineage resistant to the major predatory vibriophage ICP1, which alongside other phages, is thought to restrict cholera epidemics and has potential for use in prophylaxis. Secondly, a unique set of genes on the *Vibrio* seventh pandemic island II encodes an unusual modification-dependent restriction system targeting phages with modified genomes, and a new member of the Shedu defence family that defends against vibriophage X29. Taken together, we propose that these anti-phage defence systems have likely contributed to the success of a major epidemic lineage of the ongoing seventh cholera pandemic.

25 The ability of lytic bacteriophages to rapidly devastate bacterial populations has driven the evolution
26 of multiple layers of defence, including a diverse array of specialised anti-phage defence systems[1].
27 Bacteriophages also have the potential to affect bacterial pathogenesis, as exemplified by the cholera
28 toxin-encoding prophage CTXΦ[2]. Moreover, bacteriophage predation is thought to limit the duration
29 and severity of cholera epidemics, as well as affecting individual patient outcomes[3-6]. Sampling of
30 cholera patients has revealed that the O1 El Tor strains of *Vibrio cholerae* responsible for the ongoing
31 seventh cholera pandemic (7PET) consistently co-occur with three lytic phages ICP1, 2 and 3, with ICP1
32 being most frequently isolated[7,8]. Furthermore, the demonstration that a cocktail of ICP1-2-3 can
33 prevent cholera in animal infection models has led to renewed interest in using phages as a
34 prophylactic treatment[9]. There is therefore an urgent need to understand the mechanisms by which
35 *V. cholerae* defends against these and other viruses.
36 Since 1961 7PET strains have spread out from the Bay of Bengal in a series of three distinct but
37 overlapping waves[10]. Importantly, from Wave 2 onwards strains acquired SXT/R391 integrative and
38 conjugative elements (SXT-ICE), which in addition to carrying multiple antibiotic resistance genes,
39 encode a variable anti-phage defence hotspot that in the globally dominant SXT-ICE harbours either
40 BREX or Restriction-Modification systems active against ICP1-3[10,11]. Additionally, a family of viral
41 satellites, the Phage-inducible chromosomal island-like elements (PLE), also occur sporadically and
42 specifically parasitise ICP1 infection to mediate their own transmission[12,13]. Notably, these elements
43 exemplify the co-evolutionary arms race of defence and counter-defence between bacterial hosts and
44 their viral predators, with the emergence of resistant ICP1 phages that can overcome these defence
45 mechanisms selecting for either alternative SXT-ICE carrying new defence systems or new PLE
46 variants[11,14]. In contrast, how 7PET strains that lack SXT-ICE/PLE defend against these phages remains
47 unknown. Given their ubiquitous nature and ability to shape epidemics, we hypothesised that these
48 strains likely contained additional defence systems with activity against ICP1-3.
49

50 **WASA-1 prophage renders Peruvian strains resistant to ICP1**

51 To test this hypothesis, we challenged a set of intensively studied wave 1 strains that lack SXT-ICE/PLE
52 with a well-characterised collection of ICP1-3 phages that utilise the O1-antigen (ICP1/3) and OmpU
53 (ICP2) as receptors[7,15,16]. All strains exhibited the expected sensitivities to ICP2 and ICP3 (Fig. 1a and
54 Extended Data Fig. 1a-b). Unexpectedly, however, the widely used model strain A1552 – a Peruvian
55 isolate – was completely resistant to all 16 tested ICP1 isolates spanning a twenty-seven-year period,
56 including the most recent isolates from the Democratic Republic of the Congo[17], displaying a 10^5-fold
57 reduction in plaque formation (Fig. 1a and Extended Data Fig. 1a-e). Notably, the contemporary
58 Peruvian strains C6706 and C6709 also behaved similarly. Interestingly, although zones of lysis were
59 still observed at the highest concentrations of phage tested, re-streak tests revealed that these spots
60 contained little-to-no viable particles (Extended Data Fig. 1c), suggesting that ICP1 propagation is
61 significantly impaired and that these lysis zones represent 'lysis from without'[18]. Indeed, liquid
62 replication assays comparing A1552 with the non-Peruvian strain E7946, showed that although
63 genome injection proceeded similarly in both strains, in contrast to the robust replication observed
64 with E7946, ICP1 was completely unable to replicate on strain A1552 (Extended Data Fig. 1d). ICP1
65 resistance in strain A1552 was independent of the *Vibrio* pathogenicity islands (VPI-1/2) and the *Vibrio*
66 seventh pandemic islands (VSP-I/II), which together harbour multiple known anti-viral defence
67 systems[19-26] (Extended Data Fig. 1e). Moreover, the ICP1-resistant strains encode the same repertoire
68 of known defence systems as the ICP1-sensitive strains (Supplementary Table 1), suggesting that a
69 novel as yet unrecognised defence system(s) is likely responsible for ICP1 resistance.

70 The Peruvian strains are members of the West African South American (WASA) lineage of 7PET
71 *V. cholerae*[10], which was responsible for a massive cholera epidemic that started in Peru in 1991, before
72 spreading rapidly throughout Latin America, resulting in over 1.2 million cholera cases and
73 approximately 12,000 deaths[27]. Interestingly, phylogenetic analysis has shown that these strains
74 originated in West Africa, where they acquired two genetic signatures that define the WASA lineage:
75 (i) a novel set of genes on VSP-II and (ii) the WASA-1 prophage[10,28-31]. Since deletion of VSP-II had no
76 effect on ICP1 resistance we tested strains deleted for WASA-1. Strikingly, this abolished defence

77 against ICP1 in all tested Peruvian strains, and restored ICP1 replication to levels similar to those of a
78 susceptible control (Fig. 1b-e and Extended Data Fig. 1b). Moreover, introducing WASA-1 into non-
79 WASA lineage strains rendered them ICP1 resistant (Extended Data Fig. 1f).
80
81 **WonAB system is responsible for ICP1 defence**
82 The WASA-1 prophage is highly conserved throughout all WASA lineage strains[10,30], and interestingly,
83 is also found in diverse *Vibrio* species (Fig. 1b, Extended Data Fig. 2a and Supplementary Table 2).
84 WASA-1 displays a conserved core genome encoding proteins involved in capsid/tail biogenesis, DNA
85 replication and a recombinase (Fig. 1b). To determine the gene(s) responsible for ICP1 defence, we
86 used an existing RNA-seq dataset[32] to identify WASA-1 genes expressed under laboratory conditions,
87 and then screened truncations of these regions for loss of protection (Extended Data Fig. 2b). This
88 revealed a 2-gene operon (A1552VC_01233-34) encoding an ATPase and a hypothetical protein,
89 downstream of a conserved putative transcriptional regulator (A1552VC_01232) (Fig. 1b). For the
90 reasons outlined below we have renamed this operon WASA OLD-ABC ATPase Nuclease, WonAB.
91 Strikingly, deletion of *wonAB* abolished protection against ICP1. Moreover, ectopic expression of
92 *wonAB* complemented the Δ*wonAB* deletion and conferred complete protection to ICP1-sensitive non-
93 WASA strains (Fig. 1d-e). Importantly, both genes were required for protection indicating that
94 production of WonAB is both necessary and sufficient for anti-phage activity (Fig. 1f). Notably, although
95 WonAB is unique to the WASA-1 prophage found in *V. cholerae*, known defence systems could also be
96 found at the same locus in other non-cholerae WASA-1 (Supplementary Table 2), consistent with the
97 observation that prophages often carry anti-phage defence systems to increase the fitness of their
98 bacterial hosts[33-35].
99 Bioinformatic analysis revealed that WonA is an ATP-binding cassette (ABC) ATPase with a
100 predicted core β-barrel like ATPase fold characteristic of the ABC-ATPase clade[36]. Motifs required for
101 ATP binding and hydrolysis (Walker A, Q-loop, ABC-signature, Walker B, D-loop and H-loop) were
102 readily identifiable (Fig. 1g and Extended Data Fig. 3a). Moreover, structural modelling confidently

103 predicted that WonA forms a dimer, in which these motifs are positioned at the dimer interface to
104 form the composite ATP-binding sites typical of ABC-ATPases[36] (Fig. 1g, Extended Data Figs. 3b and 4a-
105 b). In contrast, WonB is predicted to encode a variant of the PD-(D/E)xK nuclease fold, with the highly
106 conserved active site residues clustered together[37] (Fig. 1g and Extended Data Fig. 3c-d). Variants
107 designed to disrupt either WonA ATP-binding/hydrolysis (K34A; R182A; E300A; H333A) or WonB
108 nuclease activity (K71A) all abolished protection against ICP1, despite mostly being produced at similar
109 levels to the WT control (Fig. 1h and Extended Data Fig. 3e). Interestingly, Western blotting showed
110 that inactivating WonA ATPase activity resulted in the loss of WonB, suggesting that WonA regulates
111 or otherwise affects the stability of WonB (Extended Data Fig. 3e). Indeed, the two proteins are
112 predicted to form a complex, with WonB binding to a surface created by the dimerised C-terminal
113 extensions of WonA (Fig. 1g and Extended Data Fig. 4a-d).

114 Homologues of WonAB are found in diverse classes of mainly Gram-negative bacteria and
115 overall were present in 0.43% of bacterial genomes examined (Extended Data Fig. 3f and
116 Supplementary Table 3). Notably, when expressed in *Escherichia coli* WonAB displayed robust activity
117 against all members of the *Vequintavirinae* subfamily of the BASEL bacteriophage collection[38],
118 indicating that WonAB activity is not limited to ICP1 (Extended Data Fig. 5). Interestingly, WonA ATPase
119 motifs display deviations typical of the overcoming lysogenisation defect (OLD) family of ABC-
120 ATPases[36,39] (Extended Data Fig. 3a). However, members of this family such as OLD, Gabija, PARIS and
121 the related Septu, are distinct from WonA in both structure and domain composition[39-44]. In contrast,
122 WonAB appears to be closely related to an operon encoding a predicted OLD-ABC ATPase and a novel
123 version of the restriction-enzyme fold (Extended Data Fig. 4), detected during a recent comprehensive
124 *in silico* survey of ABC-ATPases[36]. Moreover, homologues of this operon are found in 0.96% of bacterial
125 genomes and encompass all detected homologues of WonAB (Supplementary Table 3). Furthermore,
126 WonAB also shows similarity to operons with a similar organisation such as PD-T4-4 that have also
127 recently been identified (Extended Data Fig. 4), albeit with variations in the Insert 1/2 regions and C-
128 terminal extensions of the ATPase, and in some cases a distinct nuclease[34,45]. Taken together, these

129 data suggest that WonAB is part of a larger as yet uncharacterised family of ABC-ATPase sensors that
130 are paired with nuclease effectors.
131
132 **ICP1 defence occurs via lysis-independent abortive infection**
133 To gain insights into how WonAB mediates ICP1 defence we monitored the growth kinetics of ICP1-
134 infected cells at different multiplicities of infection (MOI), in the absence and presence of WASA-1 (Fig.
135 2a). This revealed that WonAB provides robust protection against ICP1 at low MOI when only a subset
136 of cells is initially infected. In contrast, infection at high MOI, when most cells are simultaneously
137 infected, resulted in a growth arrest (Fig. 2a). This phenotype is characteristic of abortive infection,
138 wherein individual cell viability is sacrificed prior to the completion of phage replication to protect the
139 surrounding bacterial population[46]. Indeed, time-lapse microscopy showed that while both WT and
140 ΔWASA-1 cells swell upon infection, cells of the ΔWASA-1 go on to lyse within ~20min, whereas WT
141 cells remain in this swollen state without lysing for the 60min duration of the experiment (Fig. 2b,
142 Extended Data Fig. 6 and movie 1). Moreover, these non-growing cells persisted in an intact state for
143 several hours before eventually undergoing lysis (Extended Data Fig. 7a-b). During this time ICP1-
144 infected cultures rebounded due to the selection of spontaneous O1-antigen mutants (Extended Data
145 Fig. 7c), as has been previously described[7]. Importantly, this is likely an *in vitro* phenomenon since O1-
146 antigen mutants are attenuated for virulence in animal infection models[47].
147 Efforts to isolate either a spontaneous or an evolved ICP1 escape mutant able to overcome
148 WonAB have so far proved unsuccessful. Therefore, to study the mode of action of WonAB in more
149 detail we investigated different stages of the ICP1 lifecycle in the absence and presence of WASA-1[8,48].
150 First, quantitative-PCR showed that ICP1 DNA replication proceeds similarly in both strain
151 backgrounds, albeit with a 2.7-fold defect in the WT background, indicating that WonAB neither
152 restricts ICP1 DNA on entry nor prevents the initiation of DNA replication (Fig. 2c). Second, microscopy
153 revealed that upon infection the nucleoids of both strains undergo dramatic changes in morphology
154 by 4min post-infection, with the nucleoid frequently appearing to contract along its long axis, likely

155 representing the action of ICP1-encoded nucleases and host-cell takeover[48,49] (Fig. 2d). Notably,
156 whereas ΔWASA-1 cells then rapidly went on to lyse, DNA in WT cells persisted in a highly compacted
157 state and went on to form toroidal structures, suggesting that WonAB does not act by simply degrading
158 DNA. Third, microscopy of ICP1-infected cells producing a fluorescent protein fusion to the ICP1 major
159 capsid protein revealed robust capsid assembly, lysis and release in the ΔWASA-1 background (Fig. 2e-
160 g). In contrast, capsid assembly was largely absent in WT cells (Fig. 2f). Taken together, these results
161 show that WonAB does not prevent the initial damage inflicted by ICP1, and suggest that WonAB is
162 activated after the initiation of ICP1 DNA replication and prevents progression to structural protein
163 assembly.
164
165 **WonAB activation shuts down cell growth by inhibiting translation**
166 The data so far are consistent with WonAB aborting ICP1 infection via a lysis-independent mechanism
167 that targets the host cell. To test whether WonAB can be artificially activated in the absence of
168 infection, we overexpressed either the *wonAB* operon or each gene individually in an otherwise WT
169 background (Fig. 3a and Extended Data Fig. 8a). While *wonAB* and *wonA* had no apparent phenotype,
170 WonB overproduction was highly toxic, resulting in a growth arrest and a rapid loss in viability, with
171 >99% of cells non-viable within 30min (Fig. 3a-c and Extended Data Fig. 8a). Furthermore, toxicity was
172 dependent on WonB nuclease activity since the WonB[K71A] variant was non-toxic (Fig. 3b-c and
173 Extended Data Fig. 8a). One explanation for these data could be that WonAB is a toxin-antitoxin system,
174 with WonA acting as an antitoxin to neutralise the toxicity of WonB[50]. Indeed, the DarTG toxin-antitoxin
175 system has recently been shown to have activity against ICP1[51]. Arguing against this hypothesis,
176 however, WonB overproduction was not toxic in a Δ*wonAB* background, despite being produced at
177 similar levels to the control (Fig. 3a and Extended Data Fig. 8b-c). Moreover, deletion of *wonA* or
178 inactivation of WonA ATPase activity also abolished the toxicity associated with WonB overproduction
179 (Fig. 3a and Extended Data Fig. 8b-c). Thus, these results rule out a simple sequestration mechanism
180 and suggest that WonA is either required to activate WonB or that the two proteins act together.

181 Microscopy revealed that following WonB overproduction growth-arrested cells exhibit
182 condensed nucleoids that at later stages display aberrant morphologies and are highly compacted (Fig.
183 3d and Extended Data Fig. 8d). Notably, the vast majority of cells retained DNA and purified genomic
184 DNA also remained intact (Extended Data Fig. 8d-e), indicating that toxicity does not result from
185 chromosomal DNA degradation. Since the nucleoid compaction phenotype resembled the effects of
186 antibiotics that inhibit translation[52], we investigated WonB production over time using Western
187 blotting (Fig. 3e). Remarkably, this revealed that compared to the inactivated WonB[K71A] control,
188 WonB is produced only for short time after induction, and by 30min post-induction was no longer
189 detectable. Importantly, qRT-PCR showed that *wonB* mRNA levels were induced similarly between the
190 two constructs and remained stable throughout the course of the experiment (Extended Data Fig. 8f).
191 These data suggested that (i) WonB overproduction inhibits translation and (ii) that WonB is likely
192 unstable. In agreement with these hypotheses, following inhibition of translation with
193 chloramphenicol, WonB rapidly disappeared in a Lon protease-dependent manner (Fig. 3f-g),
194 indicating that WonB is indeed unstable and subject to proteolytic degradation. Since in the absence
195 of ICP1, WonB was toxic only when produced in excess of WonA, Lon-mediated degradation likely
196 functions as a safety mechanism to reduce WonB accumulation and hence prevent auto-immunity.
197 Collectively, these results support a model whereby upon activation WonAB aborts phage infection by
198 inhibiting translation, and thus prevents the progression of the ICP1 lifecycle. Notably, although
199 WonAB aborts the infection, cells are likely already irreversibly damaged by ICP1 during the initial
200 stages of the infection. Furthermore, since the growth-arrest upon WonB overproduction does not
201 result in genomic DNA degradation, these results suggest that the target of WonB nuclease activity
202 could be a rRNA or tRNA.
203
204 **VSP-II^{WASA} carries two distinct anti-phage defence systems**
205 The second genetic signature of the WASA lineage is a unique variant of VSP-II (Fig. 4a), wherein the
206 chemotaxis gene cluster from the prototypical VSP-II is replaced by a set of three novel genes
207 (A1552VC_00274-76) and a frame-shifted transposase gene[10,28,53]. Although these genes are not

208 predicted to be part of a known defence system, and lacked activity against ICP1-3, bioinformatic
209 analysis revealed that they encode proteins with domains characteristic of defence systems (see
210 below). Consistent with this, when this cluster was expressed in *E. coli* we observed anti-phage activity
211 against several major groups of the BASEL collection (Fig. 4b and Extended Data Fig. 9a). As outlined
212 below, genetic dissection revealed that this cluster encodes two independent systems, with the two-
213 gene operon VC_00274-75 encoding the GmrSD-like Type IV REase of WASA strains, GrwAB (Fig. 4c-e)
214 and VC_00276 encoding the *V. cholerae* Shedu, *Vc*SduA (Fig. 4f-h).
215
216 **GrwAB is a two-component modification-dependent restriction system**
217 GrwAB showed potent anti-phage activity against all members of the *Queuovirinae* and
218 *Tevenvirinae* (*Straboviridae*), as well as some members of the *Markadamsvirinae* (*Demerecviridae*),
219 and both genes were required for protection (Fig. 4b). Interestingly, the signature feature of the
220 *Queuovirinae* and *Tevenvirinae* subfamilies is that their genomes contain hypermodified nucleobases
221 with either 7-deazaguanine modified guanosines or sugar-modified hydroxymethyl cytosines,
222 respectively, suggesting that GrwAB may recognise DNA modification[38,54,55]. In line with this
223 hypothesis, GrwAB resembles the GmrSD family of modification-dependent restriction enzymes, such
224 as GmrSD, BrxU and SspE[56-59] (Fig. 4c and Extended Data Fig. 10a-d). These are typically single protein
225 systems composed of an N-terminal DUF262 domain that likely functions as a DNA modification sensor,
226 and that uses NTP binding/hydrolysis to regulate the activity of a C-terminal His-Me nuclease domain
227 (DUF1524), which functions as an effector to target non-self DNA[56,58,60]. Indeed, GrwA is predicted to
228 share this architecture, with an N-terminal DUF262 domain containing the highly conserved QR,
229 DGQQR and FxxN motifs[56], coupled by an α-helical linker to a C-terminal DUF1524 domain containing
230 the canonical $\beta\beta\alpha$ fold and catalytic residues of the His-Me nuclease superfamily[61] (Fig. 4c and
231 Extended Data Fig. 10a-c). In contrast, and unlike known GmrSD systems, GrwB encoded by the second
232 gene contains an N-terminal DUF262 domain followed by multiple domains of unknown function (Fig.
233 4c and Extended Data Fig. 10d). Notably, variants designed to disrupt either the NTP hydrolysis of

234 DUF262 in GrwA[R81A] and GrwB[R86A], or the nuclease activity of DUF1524 in
235 GrwA[H431A]/[N521A/[N530A] all abolished anti-phage activity (Fig. 4d), indicating that GrwA and
236 GrwB function together. Indeed, structural modelling of a potential GrwAB complex supports the idea
237 that the two proteins interact (Extended Data Fig. 10e).

238 Importantly, multiple independent escaper mutants of Bas24 were obtained that overcome
239 defence by GrwAB (Extended Data Fig. 11a). These escapers all contain changes in either the active
240 site or the DNA-binding surface of DpdA – the transglycosylase that inserts the 7-deazaguanine
241 modification into the DNA – consistent with the disruption of DNA modification leading to immune
242 evasion[62] (Extended Data Fig. 11b-d). Interestingly, growth kinetics of phage-infected cultures
243 producing GrwAB lacked the growth arrest or premature lysis typical of abortive infection (Fig. 4e).
244 However, cultures did go on to exhibit moderate-to-severe lysis, which microscopy revealed was due
245 to the presence of non-dividing filamentous cells (Extended Data Fig. 12 and movie 2), suggesting that
246 either GrwAB is unable to clear the infection prior to the cell sustaining irreversible damage or that
247 the cell is subject to collateral damage during phage defence. Finally, bioinformatic analyses revealed
248 that homologues of GrwAB are found in ~1% of genomes examined (Extended Data Fig. 10f and
249 Supplementary Table 4), suggesting that GrwAB represents a new member of an emerging family of
250 two-gene GmrSD-like modification-dependent restriction enzymes that includes the recently
251 discovered TgvAB system present in *V. cholerae* VPI-2[25,26]. Similar to TgvAB, the requirement for both
252 GrwA and GrwB suggests that these proteins likely act as a complex, which could represent either a
253 novel mode of action or else a mechanism to overcome phage-encoded anti-defences. Notably,
254 despite the similarities, GrwAB has an expanded range compared to TgvAB and is also able to
255 recognise 7-deazaguanine modified DNA. Furthermore, although GrwA, TgvB and GmrSD all share a
256 similar domain architecture, except for the shared N-terminal DUF262 domain GrwB and TgvA are
257 distinct from one another[25].
258

259 ***Vc*SduA is a Shedu system with a GHKL ATPase N-terminal domain**

260 *Vc*SduA showed activity against all members of the T1-like *Drexlerviridae* family, with strong
261 protection against Bas1 (>10,000-fold), Bas03 and Bas08 (10-100-fold), while the remainder showed a
262 reduced plaque diameter that in the case of Bas03 and Bas05 was drastic (Fig. 4b and Extended Data
263 Fig. 9b). Sequence analysis and structural modelling showed that *Vc*SduA encodes an N-terminal GHKL
264 (Gyrase, Hsp90, Histidine Kinase, MutL) ATPase domain (HATPase_c) containing the highly conserved
265 motifs I-IV that define this ATPase superfamily[63,64], followed by a C-terminal PD-(D/E)xK nuclease
266 domain (DUF4263) that is also found in the Shedu defence system[20,65,66] (Fig. 4f and Extended Data Fig.
267 13a-c). Variants designed to disrupt either ATP hydrolysis *Vc*SduA[E27A] or nuclease activity
268 *Vc*SduA[K557A] both abolished anti-phage activity despite being produced at similar levels to WT
269 control (Fig. 4g and Extended Data Fig. 13d). Furthermore, growth kinetic experiments with phage-
270 infected cultures revealed similarly robust protection at all tested MOIs (Fig. 4h), consistent with
271 *Vc*SduA targeting and restricting the phage directly while preserving the viability of the host cell.

272 Proteins with a similar domain organisation to *Vc*SduA were previously annotated as
273 paraMORC3, and have recently been proposed to be part of the Shedu defence system family due to
274 the presence of the signature Shedu domain DUF4263[64,65]. Indeed, Shedu has recently been re-
275 classified as consisting of a shared nuclease domain with diverse N-terminal regulatory domains (Type
276 I), including various enzymatic domains (Type I-D)[65]. Strikingly, modelling of *Vc*SduA as a dimer (Fig.
277 4f), which are typical for GHKL ATPases, confidently predicted an entwined configuration with the GHKL
278 ATPase domain sitting below a cavity formed by a clamp-like middle domain, which in other GHKL
279 family members mediates binding to DNA and protein substrates[63,67]. We therefore hypothesise that
280 the GHKL ATPase domain functions to control the activity of the C-terminal nuclease domain.
281 Interestingly, modelling of *Vc*SduA as a tetramer was not well-supported (Extended Data Fig. 13e).
282 Furthermore, *Vc*SduA homologues were present in ~1.2% of genomes examined (Extended Data Fig.
283 13f and Supplementary Table 5), though GrwAB and *Vc*SduA were rarely found together outside of *V.*
284 *cholerae*, consistent with the demonstration above that they are independent systems. Overall, these

285 data show that *Vc*SduA is a newly identified member of the Shedu family and the first validated
286 member of the type I-D class.
287
288 **_Vc_SduA protects _V. cholerae_ against vibriophage X29**
289 Next, to determine whether GrwAB and *Vc*SduA were functional in their native *V. cholerae* host, we
290 first searched the NCBI virus database for vibriophages with modified genomes that might be targeted
291 by GrwAB (see methods). However, no such phage targeting *V. cholerae* were identified
292 (Supplementary Table 6). We therefore screened a collection of phages from the Félix d'Hérelle
293 Reference Center for Bacterial Viruses, focussing on phage X29[68] as we determined that it requires the
294 O-antigen for infection (Fig. 5a). Importantly, Darracq *et al.*, recently showed that the VSP-II encoded
295 DdmABC defence system[24] protects *V. cholerae* against X29[69]. Indeed, deletion of *ddmABC* in the non-
296 WASA 7PET strains tested here was sufficient to fully restore X29 plaque formation (Fig. 5b). In
297 contrast, deletion of *ddmABC* in the WASA-lineage strains A1552 and C6706 had no effect (Fig. 5b),
298 raising the possibility that the LAT-1 encoded defence systems of VSP-II^{WASA} were active against X29.
299 Consistent with this idea, while deletion of *grwAB* or *VcSduA* alone had no effect, deletion of either
300 the entire LAT-1 region or *VcSduA* alone in a Δ*ddmABC* background restored X29 plaque formation to
301 levels comparable to that of a complete VSP-II deletion (Fig. 5c). Furthermore, ectopic expression of
302 *VcSduA* complemented the Δ*ddmABC*Δ*VcSduA* deletion and conferred complete protection against
303 X29 in non-WASA strains deleted for *ddmABC* (Fig. 5d-e). Collectively, these data show that *Vc*SduA is
304 active in its native host organism at native expression levels, and show that WASA lineage strains have
305 two distinct mechanisms to defend against phage X29.
306
307 **Discussion**
308 The main discovery of this work is that the two unique genetic signatures (WASA-1 and VSP-II^{WASA}) of
309 the WASA lineage encode three novel antiviral defence systems: WonAB, GrwAB, *Vc*SduA. Previously,
310 these elements have primarily been used as a molecular signature to track the origins of these

311 strains[10,28-30,70], but their significance for the success of the lineage and the Latin American cholera
312 epidemic has remained unknown. Here we demonstrate that combined these systems have broad
313 activity against diverse bacteriophage families and target two-thirds of the isolates in the BASEL
314 bacteriophage collection, including those with highly modified genomes. Importantly, we also show
315 that in the native *V. cholerae* host, the WonAB system carried on the WASA-1 prophage renders strains
316 resistant to ICP1 - the major predatory phage of pandemic *V. cholerae*[8]. Given the ongoing arms race
317 between *V. cholerae* and ICP1[11,14] and the suggested role of ICP1 predation in cholera epidemics[3,4,6,7],
318 it is therefore reasonable to assume that this would have provided a significant selective advantage
319 to the lineage. Nevertheless, since WonAB can also target other phages, then together with the
320 systems carried on VSP-II^{WASA}, this selective advantage may have been against phages other than ICP1.
321 Indeed, the VSP-II^{WASA}-encoded *Vc*SduA system protects WASA lineage strains against vibriophage
322 X29, a myovirus that was originally isolated from a cholera patient in India in 1927[68,71]. Notably,
323 spacers targeting X29 are abundant in the CRISPR-Cas systems present in classical 6th pandemic and
324 non-7PET strains[72-74], suggesting that X29 (or related phages) may be commonly encountered.
325 Interestingly, since *Vc*SduA shares redundancy with DdmABC it could potentially serve to protect
326 against X29 variants that have evolved DdmABC-resistance. However, given *Vc*SduA activity against
327 *Drexlerviridae* in *E. coli* it is equally possible that it functions primarily against other non-DdmABC
328 sensitive phages.

329 Prior to the start of the epidemic in 1991, Latin America had been free from pandemic cholera
330 for almost 100 years[27,75]. However, following the introduction of the WASA lineage from West Africa
331 in the late 1980's, an explosive cholera epidemic spread rapidly throughout Latin America, with
332 >500,000 cases in Peru alone in 1991-92, and ongoing outbreaks continuing until 2001[10,27,30,31,75,76].
333 Given our findings we therefore propose that the combined activities of the defence systems encoded
334 on WASA-1 and VSP-II^{WASA} directly contributed to the success of the WASA lineage and envisage at
335 least two possible scenarios by which this could have occurred. Firstly, the acquisition of these systems
336 in Africa could have allowed the strains to resist local vibriophages, triggering the proliferation of the
337 lineage that therefore facilitated the transfer to South America. Notably, cholera outbreaks were

338 ongoing in Western and Central Africa just prior to the start of the Latin American epidemic, and
339 intensified in the years afterwards[30,31]. Furthermore, strains containing WASA-1 and VSP-II^{WASA}
340 continued to circulate in Western/Central Africa up until the late 1990's, including in the strains
341 responsible for the 1987-1996 Angolan cholera epidemic[30,31,77]. Remarkably, we found WASA-1 (99.7%
342 identity to A1552) in a recently sequenced non-7PET *V. cholerae* strain isolated in Switzerland in 2019
343 from a patient with a travel history to Morocco[78], suggesting that WonAB-containing WASA-1
344 continues to circulate in Africa. Secondly, the defences provided by WASA-1 and VSP-II^{WASA} could have
345 played a more direct role in the transmission, for example by allowing the WASA lineage to overcome
346 an entry barrier posed by phages associated with local non-pandemic *V. cholerae* strains endemic to
347 South America that might have prevented previous introductions. In support of these proposals, the
348 ability to defend against phage predation is thought to play a key role in the observed evolution of
349 local *V. cholerae* lineages, which then go on to be successful before subsequently being replaced[11,14].
350 Indeed, the continuous antagonistic co-evolution of bacterial defences and phage encoded anti-
351 defences drives the gain and loss of defence systems in natural *vibrio* populations, with such defences
352 often encoded on mobile genetic elements (MGE) and accounting for a large proportion of the
353 accessory genome[18,79]. Thus, while 7PET strains are typically considered to be clonal based on the
354 phylogeny of the core genome, closely related-strains can harbour diverse MGEs encoding defence
355 systems that vary over time in response to the dominant phages[11,14]. This, together with the results
356 presented here, reinforces the need to consider the role of the accessory genomes in the success of
357 novel lineages and therefore understanding their pandemic potential. Finally, while further work will
358 be necessary to decipher the mechanistic details of the newly discovered defence systems, this work
359 provides new insights into the evolution of one of the major epidemic lineages of the seventh cholera
360 pandemic.

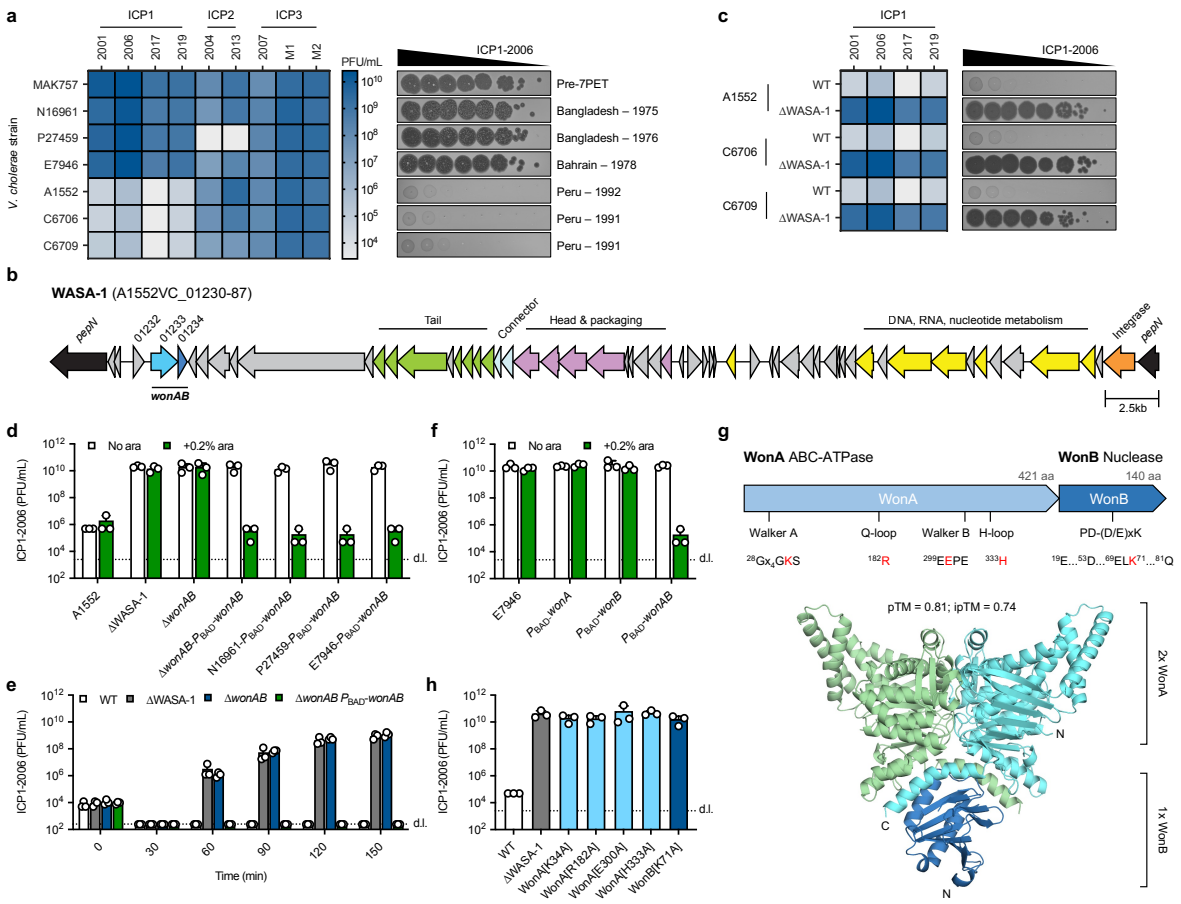

Fig. 1. WonAB carried on WASA-1 prophage renders WASA lineage ICP1 resistant. (**a**) Heat-map showing mean plaque-forming units (PFU/mL) of diverse ICP1-3 isolates determined by plaque assays on wave 1 *V. cholerae* strains, as compared to a pre-7th pandemic control (MAK757), shown alongside 10-fold serial dilution plaque assays of ICP1-2006. Data represent the results of three independent repeats. Strain P27459 encodes a naturally occurring resistant variant of the ICP2 receptor OmpU[80]. (**b**) Schematic of the WASA-1 prophage highlighting *wonAB* and genes with predicted functions in prophage biology. (**c**) Heat-map showing mean PFU/mL of diverse ICP1 isolates determined by plaque assays on Peruvian *V. cholerae* strains in WT and ΔWASA-1 backgrounds, determined as in (**a**). (**d**) Plaque assay showing the effects of ΔWASA-1, Δ*wonAB* and *wonAB* complementation in strain A1552 on ICP1-2006 PFU/mL alongside the effect of producing WonAB in non-WASA strains. (**e**) Replication assay showing change in PFU/mL over time following infection of the indicated A1552 cultures with *c.a.* 10^3-10^4 PFU of ICP1-2006. (**f**) Plaque assay showing effect of E7946 derivatives producing either WonA, WonB or WonAB on ICP1-2006 PFU/mL. Where indicated, strains in (**d-f**) contain a chromosomally integrated transposon carrying the arabinose-inducible P_{BAD}- promoter, induced by the addition of 0.2% arabinose. (**g**) AlphaFold3 predicted structure of the putative WonAB complex shown below schematic (top) indicating the conserved motifs. Residues targeted by site-directed mutagenesis are highlighted in red. (**h**) Plaque assay testing the effect of WonA and WonB site-directed variants expressed from their native locus on ICP1-2006 PFU/mL. Bar charts show the mean + s.d. from 3 independent repeats. d.l. = detection limit.

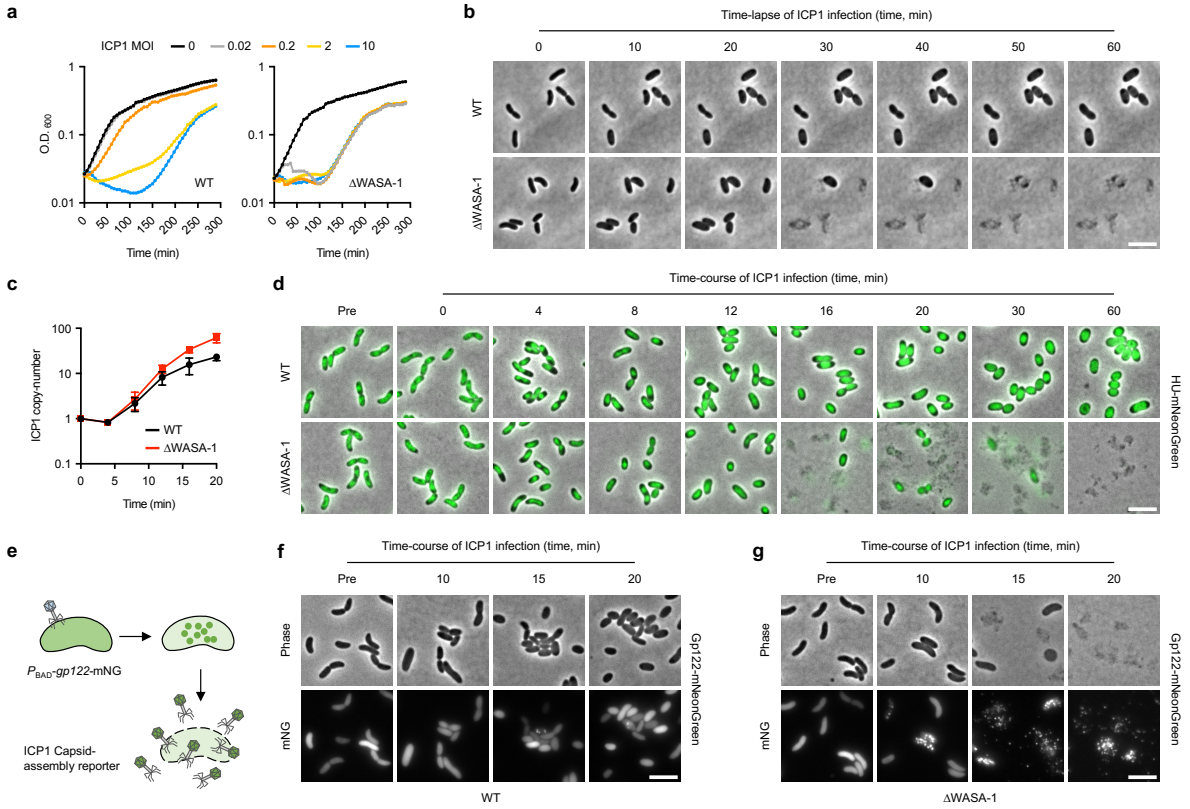

Fig. 2. WonAB protects cells by lysis-independent abortive infection. (**a**) Growth kinetics of *V. cholerae* strain A1552 in the presence (WT) and absence of WASA-1 (ΔWASA-1), with either no phage or infected at time 0 with ICP1-2006 at the indicated MOI. Data are representative of three independent repeats. (**b**) Time-lapse microscopy comparing exponentially growing cells of *V. cholerae* A1552 WT and ΔWASA-1 strains after infection with ICP1-2006 at MOI 5. (**c**) Fold-change in ICP1-2006 genome copy number relative to time 0, as determined by qPCR, after infection of either WT or ΔWASA-1 strains with ICP1-2006 at MOI 0.1. (**d**) Time-course microscopy snapshots comparing cell morphology and cellular DNA content, as monitored by a HU-mNeonGreen fusion, in WT and ΔWASA-1 backgrounds following infection with ICP1-2006 at MOI 5. (**e-g**) Time-course microscopy snapshots comparing ICP1 capsid assembly, as monitored by the incorporation of a host-cell produced mNeonGreen (mNG) fusion to the ICP1 major capsid protein Gp122 (**e**), in either WT (**f**) or ΔWASA-1 (**g**) backgrounds, following infection with ICP1-2006 at MOI 5. All images are representative of the results of three independent experiments. Scale bars = 5 µm.

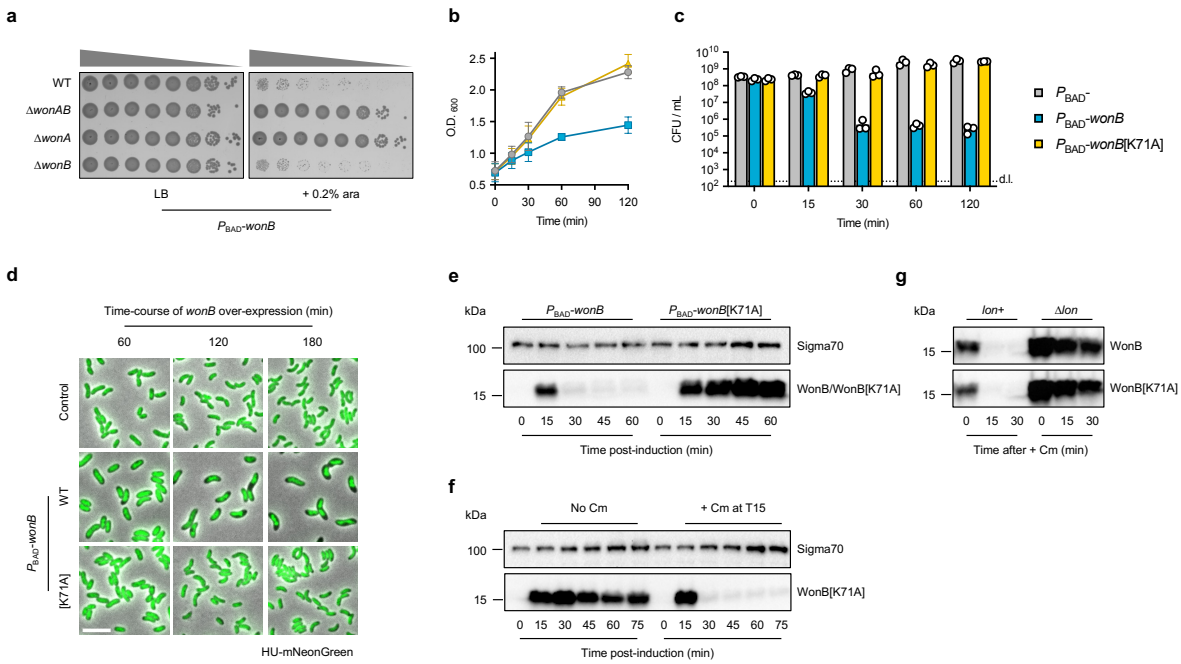

Fig. 3. WonAB activation shuts down cell growth by inhibiting translation. (**a**) Toxicity assay evaluating the growth of 10-fold serial dilutions of *V. cholerae* strain A1552 cultures and the indicated derivatives on solid media, in the absence (LB) and presence (+ 0.2% ara) of WonB overproduction. (**b**-**c**) Toxicity assay evaluating the growth kinetics (**b**) and cell viability (**c**) of exponentially growing cultures in liquid media upon WonB overproduction following induction at time 0, as compared to a negative control strain and a strain overproducing the inactive WonB[K71A] variant. (**d**) Time-course microscopy snapshots showing the effect of WonB overproduction on cell morphology and cellular DNA content, as monitored by a HU-mNeonGreen fusion, compared to a negative control strain and a strain overproducing the inactive WonB[K71A] variant. Scale bar = 5 µm. (**e**) Western blot showing protein levels of WonB and WonB[K71A] over time following induction in exponentially growing cells at time 0. Predicted molecular mass of WonB, 16.1 kDa. Sigma70, was used as a loading control (**f**) Western blot showing protein levels of WonB[K71A] over time following induction in exponentially growing cells at time 0, in the absence and presence of chloramphenicol (Cm), added at 15min (T15). (**g**) Western blot showing protein levels of WonB and WonB[K71A] over time following chloramphenicol (Cm) addition, in the presence (*lon*+) and absence of Lon protease (Δ*lon*). Overexpression of genes in (**a**-**g**) was done from a chromosomally integrated transposon carrying the arabinose-inducible P_{BAD}- promoter, induced by the addition of 0.2% arabinose. Charts show mean values, error bars show s.d. All images, charts and blots are representative of the results of three independent experiments.

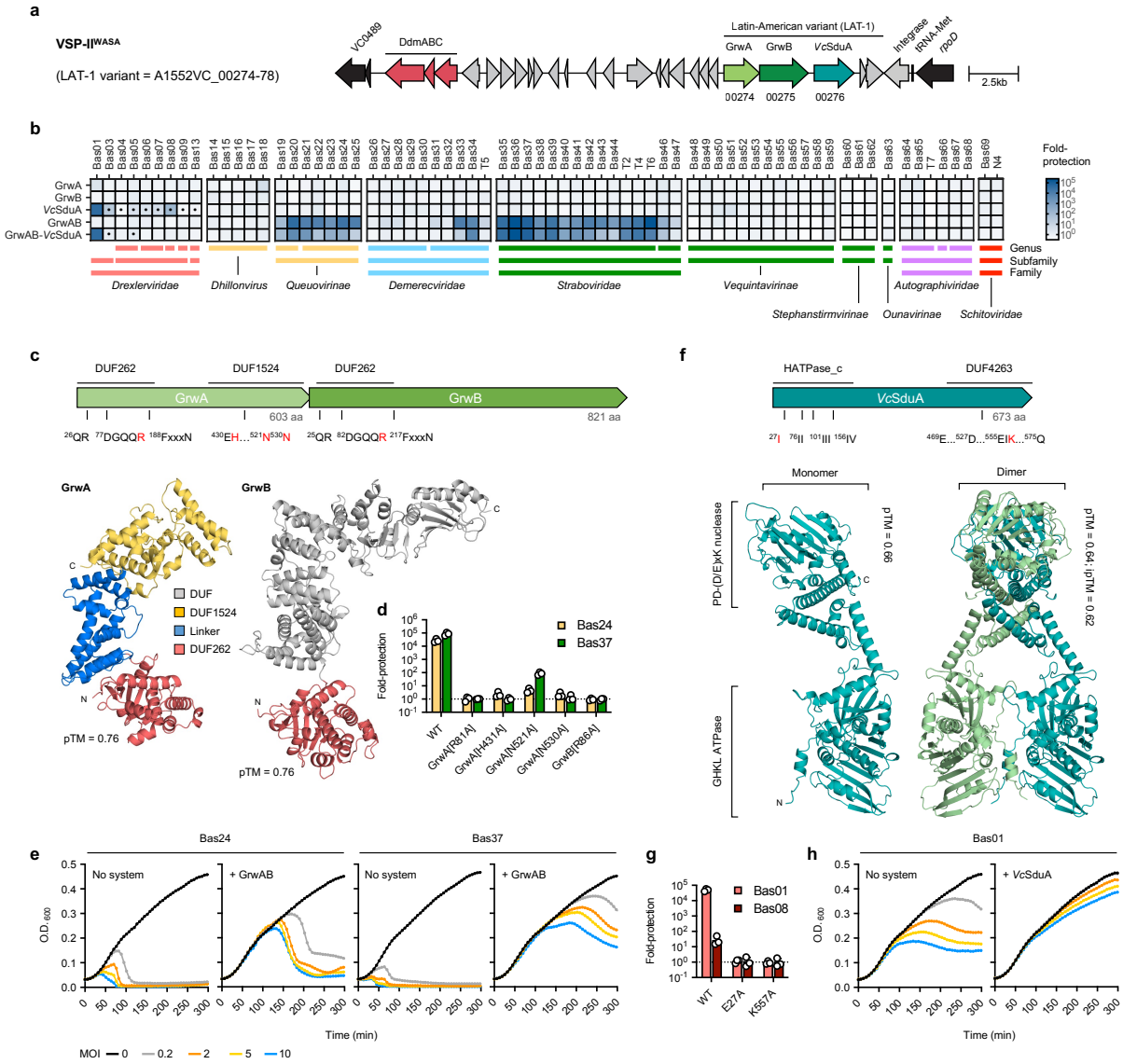

Fig. 4. VSP-II^{WASA} variant encodes two distinct anti-phage defence systems. (**a**) Schematic of VSP-II^{WASA} highlighting the LAT-1 variant present in the WASA lineage and the previously characterised DdmABC system. (**b**) Fold-protection against *E. coli* phages of the BASEL collection conferred by the production of the indicated systems and components in *E. coli*, compared to a negative 'no system' control. Boxes with a filled dot indicate phages exhibiting altered plaque morphology. Data represent the mean of two independent repeats. (**c, f**) Predicted structures of GrwAB (**c**) and *Vc*SduA (**f**) generated using AlphaFold3 shown below schematics (top) indicating the conserved domains and motifs identified in each system. Residues targeted by site-directed mutagenesis are highlighted in red. (**d**, **g**) Fold-protection against the indicated *E. coli* phages conferred by site-directed variants of GrwAB (**d**) and *Vc*SduA (**g**) in *E. coli*, compared to a negative 'no system' control. Bar charts show the mean + s.d. of three independent repeats. (**e**, **h**) Growth kinetics of *E. coli* cultures in the absence (No system) and presence of either GrwAB (**e**) or *Vc*SduA (**h**), with either no phage or infected at time 0 with the indicated MOI. Data are representative of three independent repeats. Systems were expressed from a chromosomally integrated transposon using the arabinose-inducible P_{BAD}- promoter. Growth media were supplemented with 0.2% arabinose.

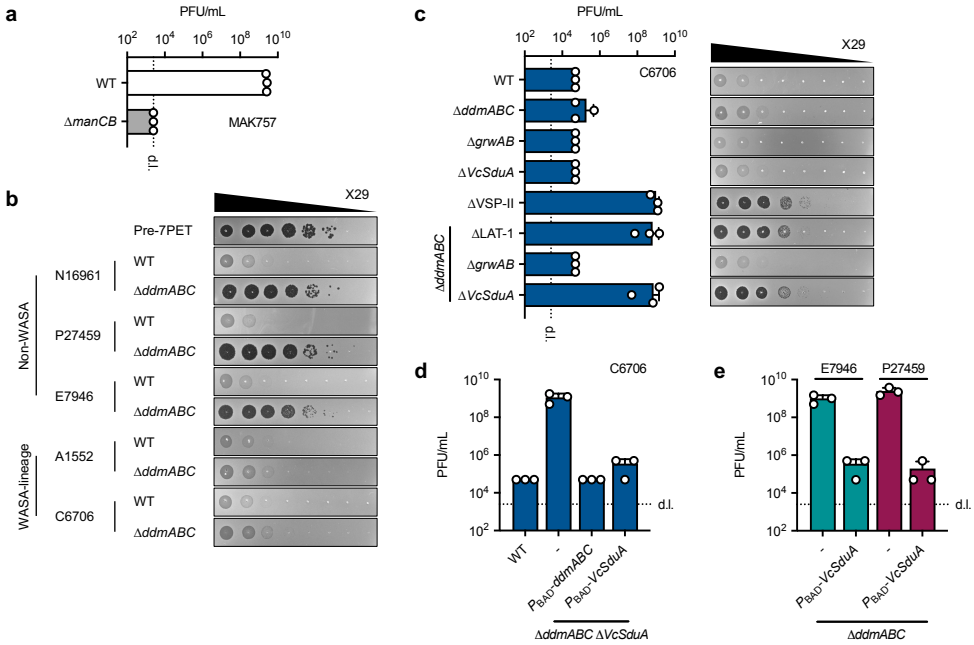

Fig. 5. *Vc*SduA protects *V. cholerae* against *vibrio* phage X29. (**a**) Plaque assay showing X29 plaque-forming units (PFU/mL) on the pre-7th pandemic strain MAK757, in the presence and absence (Δ*manCB*) of the O1-antigen. (**b**) 10-fold serial dilution plaque assays of X29 on wave 1 *V. cholerae* strains, comparing the effect of deleting *ddmABC* in non-WASA (N16961, P27459, E7946) and WASA-lineage (A1552, C6706) strains, below a pre-7th pandemic control (MAK757). (**c**) Plaque assay showing X29 PFU/mL obtained on C6706 derivates deleted for combinations of *ddmABC* with ΔLAT1 (Δ*grwAB-VcSduA*), Δ*grwAB* and Δ*VcSduA*, alongside representative images of each 10-fold serial dilution plaque assay. Note that strain C6706 was used in these assays because the rifampicin antibiotic resistance marker in strain A1552 partially interferes with X29 infection. (**d-e**) Plaque assays testing the ability of *Vc*SduA production to complement X29 protection in a C6706Δ*ddmABC*Δ*VcSduA* background (**d**) and in Δ*ddmABC* backgrounds of the non-WASA linage strains E7946 and P27459 (**e**). Bar charts show the mean + s.d. from 3 independent repeats. d.l. = detection limit. Images are representative of the results of three independent experiments.

450 **Materials and Methods**

451 **Bacterial strains, plasmids and bacteriophages**

452 The bacterial strains, plasmids, bacteriophages and defence systems used in this work are detailed in
453 Supplementary Table 7. The primary *V. cholerae* strain used throughout this work, A1552, is an O1 El
454 Tor (Inaba) strain isolated from a patient in 1992 following an outbreak of cholera linked to a
455 commercial airline flight between Lima, Peru and Los Angeles, California, U.S.A[81-83]. The primary *E. coli*
456 strain used throughout this work is the non-arabinose metabolising strain MG1655Δ*araCBAD*[84]. *E. coli*
457 strains S17-1λ*pir* and MFD*pir* were used for cloning and bacterial mating with plasmids containing the
458 conditional R6K origin of replication[85,86].

459

460 **Growth conditions**

461 Bacteria were cultured either in Lysogeny broth (LB-Miller; 10 g/L tryptone, 5 g/L yeast extract, 10 g/L
462 NaCl; Carl Roth, Switzerland) with shaking at 180rpm or on LB + 1.5% agar plates, at 37°C.
463 Transformation of *V. cholerae* was done on chitin powder (Alfa Aesar via Thermo Fisher, U.S.A)
464 suspended in half-concentrated Instant Ocean medium (Aquarium Systems) and sterilised by
465 autoclaving. Thiosulfate citrate bile salts sucrose (TCBS) agar plates were used for counter-selection
466 against *E. coli* following bacterial mating (Sigma-Aldrich). SacB-based counter-selection for allelic
467 exchange was done on NaCl-free media containing 10% sucrose. Counter-selection of *pheS**-carrying
468 strains (see below) was done on LB agar plates supplemented with 20 mM 4-chloro-phenylalanine
469 (cPhe). Ampicillin (Amp; 100 µg/mL), chloramphenicol (Cm; 2.5 µg/mL), gentamicin (Gent; 25-50
470 µg/mL), kanamycin (Kan; 75 µg/mL), streptomycin (Strep; 100 µg/mL) and rifampicin (Rif; 100 µg/mL)
471 were used for selection, as required. Growth of MFD*pir* was supported by the addition of 0.3 mM
472 diaminopimelic acid (DAP; Sigma-Aldrich). Unless stated otherwise, genes under control of the P_{BAD}-
473 promoter were induced by supplementing growth media with 0.2% L-arabinose.

474

475 **Strain construction**

476 Genetic engineering of *V. cholerae* was done using natural competence for transformation to
477 introduce deletions marked with antibiotic resistance genes[87], which when necessary were removed
478 using FLP recombination (TransFLP;[88,89]). Alternatively, antibiotic cassettes linked to the modified
479 phenylalanyl-tRNA synthetase *pheS** (*pheS*[A294G/T251A]) were removed by natural transformation
480 using the Trans2 method[90]. Scar-less, marker-less modifications were introduced using allelic
481 exchange with derivatives of the counter-selectable plasmid pGP704-Sac28[91]. A mini-Tn7 transposon
482 carrying *araC* and the indicated gene(s) of interest under control of the P_{BAD}- promoter was integrated
483 downstream of the *glmS* locus in *V. cholerae* and *E. coli* by introducing derivatives of pGP704-TnAraC
484 via tri-parental mating, as previously described[92]. Plasmids were constructed using either standard
485 restriction enzyme cloning or by inverse PCR, and were used exclusively as intermediates for strain
486 construction. All strains and constructs were verified by PCR, and either Sanger sequencing or Oxford
487 Nanopore Technologies (ONT)-based full plasmid sequencing (Microsynth AG, Switzerland).

488

489 ***V. cholerae* bacteriophage methods**

490 Vibriophages were propagated on *V. cholerae* strains E7946 or MAK757 (ICP1 and ICP3) and
491 E7946Δ*manCB* (ICP2). Briefly, overnight cultures were back-diluted and grown in LB at 37°C, 180rpm
492 to exponential phase (optical density at 600nm, OD_{600} *c.a.* 0.5-0.6), infected with the relevant phage
493 at a multiplicity of infection (MOI) of <0.01. Following lysis of the culture, debris was removed by
494 centrifugation (10min; 4,000 x *g*; RT), lysates passed through a 0.2µm filter, and stored at 4°C after
495 the addition of chloroform to 1%. Phage titres were determined by plaque assays on strain E7946
496 using the small-drop plaque assay on double-layer plates, as described below. To quantify ICP and X29
497 phage infections, 100µL and 10µL, respectively, of overnight culture was added to molten top-agar
498 (LB + 0.5% agar), poured on top of a bottom agar (LB + 1.5% agar), and allowed to solidify at RT. For
499 complementation of *wonAB* and *VcSduA*, cultures were grown either for 2h + 0.2% arabinose or
500 overnight with 0.02% arabinose, respectively, and the top agar was also supplemented with arabinose

501 at the respective concentration. Phages were serially-diluted (10^{-1}-10^{-8}), 4µL of each dilution spotted
502 onto plates, and allowed to dry under a laminar flow hood. Plates were imaged after overnight
503 incubation at 37°C, and the plaque-forming units (PFU/mL) enumerated. The theoretical detection
504 limit in this experiment was $2.5x10^3$ PFU/mL. In cases where no discrete plaques were observed but a
505 zone of non-specific lysis was apparent (*e.g.* ICP1 on strain A1552; Fig. 1a), the last dilution exhibiting
506 this phenotype was counted as 20 plaques. To determine whether these zones of non-specific lysis
507 resulted from phage propagation or "lysis from without" (*i.e.* lysis at high phage concentration without
508 viable phage production) re-streak tests were performed, as previously described[18]. Material from the
509 highest phage concentration spot on plaque assay plates was re-streaked onto freshly poured top agar
510 plates containing the ICP1-sensitive strain A1552ΔWASA-1.
511
512 ***E. coli* bacteriophage methods**
513 The BASEL (BActeriophage SElection for your Laboratory) collection of *E. coli* bacteriophages was
514 obtained from A. Harms, ETH Zürich[38]. Infections were quantified using the small-drop plaque assay
515 described above, with the following modifications. Briefly, overnight cultures of *E. coli*
516 MG1655Δ*araCBAD* were back-diluted 1:100 in 3mL LB + 5mM $CaCl_2$, 20mM $MgSO_4$, 0.2% arabinose
517 and grown 2h at 37°C, 180rpm to reach exponential phase, before being diluted 1:40 in molten top
518 agar, supplemented with 5mM $CaCl_2$, 20mM $MgSO_4$ and 0.2% arabinose. Phages were serially-diluted
519 (10^{-1}-10^{-8}), 5µL of each dilution spotted onto plates, and allowed to dry under a laminar flow hood.
520 Plates were imaged after overnight incubation at 37°C, and the plaque-forming units (PFU/mL)
521 enumerated. The theoretical detection limit in this experiment was $2x10^3$ PFU/mL. Fold-protection
522 was calculated as the ratio of PFU/mL on the strain of interest to that of the no system control strain
523 *E. coli* MG1655Δ*araCBAD*-TnAraC.
524

525 **Quantification of infectious ICP1 phages**

526 To monitor the production of infectious ICP1 phages, overnight cultures of the *V. cholerae* strains
527 indicated in the text were back-diluted 1:100 in 2.5mL LB in 14mL test-tubes and grown at 37°C,
528 180rpm to exponential phase (OD_{600} *c.a.* 0.5-0.6) before being infected with *c.a.* 10^3-10^4 PFU/mL of
529 ICP1-2006. Infected cultures were incubated at 37°C, 180rpm and sampled at 30min intervals for 2.5h.
530 At each time-point, 300µL culture was mixed with 30µL of chloroform, vortexed vigorously for 10s and
531 centrifuged (3min; 20,000 x *g*; RT). To determine the starting titre at time 0 samples were prepared
532 from LB only controls. Chloroform-free supernatants were transferred to new tubes, serially diluted
533 (10^0-10^{-7}) and PFU/mL enumerated by a plaque assay on plates seeded with the ICP1-sensitive *V.*
534 *cholerae* strain E7946. The theoretical detection limit in this experiment was 2.5×10^2 PFU/mL.

535

536 **Bacteriophage infection kinetics**

537 To monitor the kinetics of ICP1 infection, overnight cultures of the *V. cholerae* strains indicated in the
538 text were back-diluted 1:100 in 2.5mL LB in 14mL test-tubes and grown at 37°C, 180rpm for 1h45min
539 to exponential phase (OD_{600} *c.a.* 0.5-0.6). 180µL aliquots of cultures diluted 1:5 in pre-warmed LB were
540 added to the wells of a 96-well plate containing 20µL of ICP1-2006 at the indicated MOI (in technical
541 triplicate). Bacterial growth (OD_{600}) at 37°C with shaking was followed using a SpectraMax i3x
542 (Molecular Devices) plate reader at 6-min intervals for a total of 49 cycles. The kinetics of Bas01, Bas24
543 and Bas37 infection in *E. coli* were monitored exactly as described above, except that *E. coli* strains
544 were grown for 2h in LB + 5mM $CaCl_2$, 20mM $MgSO_4$, 0.2% arabinose and aliquots were diluted 1:10.
545 *E. coli* phages used for plate reader experiments were propagated on MG1655Δ*araCBAD*, as described
546 above.

547

548 **Microscopy**

549 Imaging was conducted using Zeiss Axio Imager M2 and Zeiss Axio Observer Z1 epifluorescence
550 microscopes, equipped with AxioCam MRm cameras and controlled by Zeiss Zen software (v.2.6 blue

551 edition). Images were captured using a Plan-Apochromat 100x/1.4-NA Ph3 oil objective, and for
552 fluorescence microscopy illumination with an HXP120 lamp. For snap-shot imaging, cells were
553 immobilized on slides coated with 1.2% (wt/vol) agarose in PBS, covered with a No. 1 coverslip. For
554 time-lapse microscopy, cells were immobilized on slides coated with 1.2% (wt/vol) agarose in either
555 LB (ICP1 infection of *V. cholerae*) or LB + 5mM $CaCl_2$, 20mM $MgSO_4$, 0.2% arabinose (Bas24 infection
556 of *E. coli*) and imaged automatically at the indicated time-points, within a temperature-controlled
557 stage-top chamber (H301-K-Frame; OKO Lab, Italy) set to 37°C with an accompanying objective-
558 heater. Images were prepared for publication using ImageJ (version 2.1.0/1.53h;
559 imagej.net/software/fiji), and where needed, drift was corrected using the HyperStackRegPlus
560 function of MicrobeJ[93].
561
562 **Time-lapse and time-course microscopy of ICP1 infection**
563 To image ICP1 infection in *V. cholerae*, overnight cultures of the strains indicated in the text were back-
564 diluted 1:100 in 2.5mL LB in 14mL test-tubes and grown at 37°C, 180rpm for 1h45min to exponential
565 phase (OD_{600} *c.a.* 0.5-0.6). For time-lapse microscopy, an aliquot of the culture was then mixed with
566 ICP1-2006 to achieve a MOI of 5, and immediately transferred to a slide and imaged, as described
567 above. For time-course microscopy, 180µL aliquots of cultures were mixed with 20µL ICP1-2006 in
568 2mL microcentrifuge tubes to achieve a MOI of 5 and incubated flat at 37°C, 180rpm. At the indicated
569 time-points, tubes were removed from the incubator and samples immediately transferred to a slide
570 and imaged, as described above. To monitor cellular DNA content, strains were used encoding a C-
571 terminal mNeonGreen fusion to the Histone-like DNA-binding protein HU (HU-mNeonGreen)
572 separated by a GSGSGS linker, and expressed from the native *hupA* locus. To monitor ICP1 capsid
573 assembly, infections were performed in strains with a chromosomally integrated transposon carrying
574 a C-terminal mNeonGreen fusion to the ICP1 major capsid protein Gp122 (Gp122-mNeonGreen),
575 separated by a GSGSGS linker, and expressed under the control of the arabinose-inducible P_{BAD}-
576 promoter. The fusion was induced by the inclusion of 0.02% arabinose in the growth media.

577

578 **Time-lapse microscopy of Bas24 infection**

579 To image Bas24 infection in *E. coli*, overnight cultures were back-diluted 1:100 in 3mL LB + 5mM $CaCl_2$,
580 20mM $MgSO_4$, 0.2% arabinose in 14mL test-tubes and grown at 37°C, 180rpm for 2h to mirror the
581 conditions used for the BASEL screen above. An aliquot of the culture was then mixed with Bas24 to
582 achieve a MOI of 10, and allowed to stand at RT for 2min before being transferred to a slide and
583 imaged.

584

585 **Quantitative PCR (qPCR) of ICP1 genome replication**

586 ICP1 genome replication was quantified by quantitative PCR (qPCR) using a protocol modified from[13].
587 Briefly, overnight cultures were back-diluted 1:100 in 2.5mL LB in 14mL test-tubes and grown at 37°C,
588 180rpm for 1h45min to exponential phase (OD_{600} *c.a.* 0.5-0.6). ICP1-2006 was then added to a MOI of
589 0.1, tubes briefly vortexed to ensure proper mixing, and a 20µL sample immediately withdrawn (t = 0)
590 and heat-inactivated at 95°C for 20min. Sampling was repeated following incubation at 37°C, 180rpm
591 for 4, 8, 12, 16 and 20min post-infection. Samples were analysed using a LightCycler 96 Instrument
592 (Roche) with SYBR Green I (Fast Start Essential DNA Green Master; Roche) to detect amplification
593 products using the ICP1-specific primers qICP12006E_148-f (ACTTTGGTGCGTGAAGAAGG) and
594 qICP12006E_148-r (ACTTGCTCACCTGAATGGTC). ICP1 genome copy number levels are presented
595 relative to t = 0, and were analysed with LightCycler 96 software v.1.1.0.1320 (Roche) with the
596 absolute quantification method using a standard curve of purified ICP1-2006 genomic DNA.

597

598 **WonB toxicity assay**

599 Overnight cultures were back-diluted to OD_{600} 0.05 in LB and grown 1h45min at 37°C, 180rpm to
600 exponential phase (OD_{600} *c.a.* 0.5-0.6), induced by the addition of 0.2% arabinose (t = 0), and
601 incubation continued for 120min. The OD_{600} of each culture was measured at t = 0, 15, 30, 60, and
602 120min. At each time point, samples were collected and processed to determine the (i) CFU/mL by

603 serial-dilution and plating on LB agar, (ii) transcript levels via qRT-PCR and (iii) genomic DNA was
604 prepared using a GenElute Bacterial Genomic DNA Kit (NA2110; Sigma-Aldrich) according to the
605 manufacturer's instructions. Samples to determine protein levels by Western blotting were collected
606 at the time-points indicated in the text and processed as described below. To determine the stability
607 of WonB protein levels over time, translation was inhibited by the addition of chloramphenicol to 200
608 µg/mL.
609
610 **Quantitative reverse transcription PCR (qRT-PCR) of *wonAB* transcript levels**
611 2mL culture samples from the WonB toxicity assay (above) were harvested by centrifugation (3min;
612 20,000 x *g*; 4°C), cell pellets resuspended in Tri-Reagent (Sigma-Aldrich), snap-frozen in a dry ice-
613 ethanol bath, and stored at -80°C. RNA extraction, cDNA synthesis, and qPCR was then performed
614 exactly as previously described[94], using a LightCycler 96 Instrument (Roche). Transcript levels are
615 presented relative to mRNA levels of the reference gene *gyrA*, and were analysed with LightCycler 96
616 software v.1.1.0.1320 (Roche) using the standard curve method. Primers used to detect *wonA and*
617 *wonB* were: qVC_01233-F (GTCCACAAGCAAACGGTAAG) and qVC_01233-R
618 (TTCTCCCATGAATACCTCGG); qVC_01234-F (ACAACTGTCTCAAAGGATCC) and qVC_01234-R
619 (GCTCAATATCCAGTCACATC).
620
621 **Western Blotting**
622 Unless stated otherwise, overnight cultures were back-diluted 1:100 and grown at 37°C, 180rpm for
623 3h. Lysates were prepared by resuspending pelleted bacteria in 2x Laemmli buffer (Sigma-Aldrich),
624 normalised to optical density (100 µL buffer per OD unit), and samples were then heated at 95°C,
625 15min. Proteins were resolved on Mini-PROTEAN TGX Stain-Free precast gels (10% or 12%, as
626 required; Bio-Rad) and transferred onto PVDF membranes using a Trans-Blot Turbo Transfer System
627 (Bio-Rad) according to the manufacturer's instructions. Membranes were blocked in 2.5% skim milk
628 in TBST (1x Tris-buffered saline with 0.1% Tween-20) with agitation at either RT for 1h or at 4°C

629 overnight. Primary antibodies were added at a dilution of 1:500 in TBST and membranes incubated at
630 RT for 1h. Membranes were then washed three times with TBST before being incubated at RT for 1h
631 with anti-rabbit IgG conjugated to HRP (A9169, Sigma-Aldrich) diluted 1:20,000 in TBST. Membranes
632 were washed as above and visualised by chemiluminescence using Lumi-Light^{PLUS} Western Blotting
633 Substrate (Roche). Primary antibodies against WonA (2210455), WonB (2210453) and *Vc*SduA
634 (2310059) were custom-raised in rabbits against synthetic peptides (Eurogentec), and their specificity
635 validated by comparing strains lacking the relevant proteins. Uniform sample loading was verified by
636 the intensity of non-specific bands on the membranes or by detection of Sigma70 (1:10,000 diluted
637 anti-Sigma70-HRP antibody from BioLegend, U.S.A).
638
639 **Identification of defence systems, protein domains, motifs and structural predictions**
640 The repertoire of known defence systems present in *V. cholerae* strains was identified using
641 DefenseFinder (v.1.2.4) and PADLOC (v.2.0.0) (accessed May 14th 2024), see Supplementary Table 1
642 for details[95,96]. Conserved protein domains were initially identified by searching the PFAM and NCBI
643 Conserved Domain Database with the MOTIF Search tool (genome.jp/tools/motif/; accessed July 22nd
644 2024), and was supplemented by remote homology searches using HHpred (PDB_mmCIF70_8_Mar,
645 default database; accessed July 22nd 2024), and structural alignments performed with DALI using
646 structural predictions generated by AlphaFold3[97-99]. The predicted template modelling (pTM) score,
647 and where appropriate, the interface predicted template modelling (ipTM) score, are shown alongside
648 each model[99]. For full confidence metrics for AlphaFold models, see Supplementary Fig. 1. Sequence
649 logos showing the conservation of motifs in each system were generated using Weblogo 3 from
650 multiple sequence alignments done using MAFFT[100,101].
651
652 **Identification and distribution of WASA-1**
653 A BLASTN search of the *V. cholerae* A1552 WASA-1 sequence (default parameters; evalue 1e-10)
654 against 45,725 bacterial genomes (NCBI, Refseq database, complete and chromosome level genomes,
655 downloaded on May 22nd 2024) revealed hits exclusively in the *Vibrio* genus. The BLASTN search was

656 therefore repeated against a database consisting of 7,624 genomes, covering all available assemblies
657 within the *Vibrio* genus (Refseq database, genomes from contig to complete level assemblies,
658 downloaded on May 30th 2024). A second complementary BLASTN search was also performed with
659 the additional max_hsps (high-scoring pair) parameter set to 1. Initial hits were then manually curated
660 to identify complete WASA-1 assemblies, as shown in Supplementary Table 2. WASA-1 conservation
661 was visualised using clinker (v.0.0.28, default parameters)[102].
662
663 **Identification and distribution of defence systems**
664 The presence of the WonAB, OLD-ABC ATPase + Novel REase, GrwAB and *Vc*SduA defence systems
665 was determined against 45,725 bacterial genomes (NCBI, Refseq database, complete and
666 chromosome level genomes, downloaded on May 22nd 2024) using MacSyFinder (v.2.1.1; default
667 parameters)[103]. To build HMM profiles, a PSI-BLAST of each component was performed against the
668 NCBI non-redundant protein sequence database (accessed in February 2023, and May 2024). The PSI-
669 blast e-value threshold was set to 1e-10 and run for three iterations, except for *Vc*SduA for which only
670 one iteration was performed due to NCBI computational constraints. Sequences were aligned using
671 MAFFT (v.7.508; --maxiterate 1000 –localpair parameters for a higher accuracy alignment) and HMM
672 profiles built using the hmmbuild function of the HMMER suite (v.3.3.2; default parameters)[101,104]. To
673 evaluate the distribution of each system in the RefSeq database used, genera represented with more
674 than 500 genomes were extracted, and the NCBI common tree tool used to create an order-level
675 phylogenetic tree showing the most represented clades, with the presence/absence of each system
676 mapped. For the full list of identified hits see Supplementary Tables 3-5.
677
678 **Isolation and characterisation of Bas24 escaper phages that overcome GrwAB**
679 Candidate escaper phages of Bas24, which appeared as spontaneous large plaques in the lowest
680 dilution of the small-drop plaque assay on strains producing GrwAB, were isolated and propagated
681 using a protocol modified from[105]. Single plaques of each candidate were resuspended in 90µL phage
682 buffer (50mM Tris-HCL pH 7.5, 100 mM $MgCl_2$, 10mM NaCl), added to 1mL exponentially growing *E.*

683 *coli* MG1655Δ*araCBAD* producing GrwAB in a 14mL test-tube and cultured at 37°C, 180rpm for 3h, at
684 which point a further 2mL of exponentially growing culture was added and incubated for 3h, before
685 phages were purified exactly as described above. As a control, a single plaque from the no system
686 control plate was picked and propagated in the absence of GrwAB production. Genomic DNA was
687 prepared using the Norgen Phage DNA Isolation Kit (Product #46850; Norgen, Canada) according to
688 the manufacturer's instructions. Whole genome sequencing was done using the Small, 200 Mbp
689 Illumina short read service on the Illumina NextSeq2000 platform (SeqCoast Genomics, U.S.A).
690 Genomes were assembled using Unicycler (v.0.5.0)[106], using short reads only as input with the
691 remaining parameters set to default, and assemblies rotated to match the Bas24 reference genome[107].
692 Genomes were aligned using MAFFT (v.7.508) and single nucleotide polymorphisms called using snp-
693 sites (v.2.5.1)[101,108].
694
695 **Search for DpdA-encoding vibriophages**
696 To identify previously described vibriophages with modified genomes, phage sequences were
697 downloaded from the NCBI virus database, with Vibrionaceae (taxid: 641) specified as the host. Using
698 the resulting 1,700 nucleotide assemblies and the NCBI tool suite (v.2.14.1) to translate the sequences,
699 a local database containing 117,034 protein sequences was generated (makeblastdb). This database
700 was then searched for homologues of DpdA from phage Bas24 using Blastp (e-value 1e-10, rest of
701 parameters to default). The resulting data are provided in Supplementary Table 6.
702
703 **Genome sequencing of Swiss WASA-1 strain N19-2759**
704 *V. cholerae* strain N19-2759 is a non-O1/non-O139 non-toxigenic travel-associated clinical isolate
705 isolated from a patient in Switzerland in 2019 (Illumina-based sequencing accession number
706 GCA_032819675.1)[78]. To obtain an assembled complete genome of strain N19-2759, genomic DNA
707 was prepared as previously described[109], sequenced using ONT-based sequencing, and assembled
708 using the software flye[110] [v. 2.9.3] (Microsynth, Switzerland).

709 **Data availability**

710 The genome assemblies of *V. cholerae* strain N19-2759 have been deposited in the NCBI GenBank
711 database under accession number GCA_046097525.1. The raw reads are available from the Sequence
712 Read Archive (SRA) under submission number SRX26909066. All other data are available in the main
713 text or the supplementary materials.

714

715 **References**

716 1 Georjon, H. & Bernheim, A. The highly diverse antiphage defence systems of bacteria. *Nat Rev*
717 *Microbiol* **21**, 686-700, doi:10.1038/s41579-023-00934-x (2023).
718 2 Waldor, M. K. & Mekalanos, J. J. Lysogenic conversion by a filamentous phage encoding
719 cholera toxin. *Science* **272**, 1910-4, doi:10.1126/science.272.5270.1910 (1996).
720 3 Faruque, S. M. *et al.* Seasonal epidemics of cholera inversely correlate with the prevalence of
721 environmental cholera phages. *Proc Natl Acad Sci U S A* **102**, 1702-7,
722 doi:10.1073/pnas.0408992102 (2005).
723 4 Faruque, S. M. *et al.* Self-limiting nature of seasonal cholera epidemics: Role of host-mediated
724 amplification of phage. *Proc Natl Acad Sci U S A* **102**, 6119-24, doi:10.1073/pnas.0502069102
725 (2005).
726 5 Jensen, M. A., Faruque, S. M., Mekalanos, J. J. & Levin, B. R. Modeling the role of bacteriophage
727 in the control of cholera outbreaks. *Proc Natl Acad Sci U S A* **103**, 4652-7,
728 doi:10.1073/pnas.0600166103 (2006).
729 6 Madi, N. *et al.* Phage predation, disease severity, and pathogen genetic diversity in cholera
730 patients. *Science* **384**, eadj3166, doi:10.1126/science.adj3166 (2024).
731 7 Seed, K. D. *et al.* Evidence of a dominant lineage of *Vibrio cholerae*-specific lytic
732 bacteriophages shed by cholera patients over a 10-year period in Dhaka, Bangladesh. *mBio* **2**,
733 e00334-10, doi:10.1128/mBio.00334-10 (2011).
734 8 Boyd, C. M. *et al.* Bacteriophage ICP1: A Persistent Predator of *Vibrio cholerae*. *Annu Rev Virol*
735 **8**, 285-304, doi:10.1146/annurev-virology-091919-072020 (2021).
736 9 Yen, M., Cairns, L. S. & Camilli, A. A cocktail of three virulent bacteriophages prevents *Vibrio*
737 *cholerae* infection in animal models. *Nat Commun* **8**, 14187, doi:10.1038/ncomms14187
738 (2017).
739 10 Mutreja, A. *et al.* Evidence for several waves of global transmission in the seventh cholera
740 pandemic. *Nature* **477**, 462-5, doi:10.1038/nature10392 (2011).
741 11 LeGault, K. N. *et al.* Temporal shifts in antibiotic resistance elements govern phage-pathogen
742 conflicts. *Science* **373**, doi:10.1126/science.abg2166 (2021).
743 12 Seed, K. D., Lazinski, D. W., Calderwood, S. B. & Camilli, A. A bacteriophage encodes its own
744 CRISPR/Cas adaptive response to evade host innate immunity. *Nature* **494**, 489-91,
745 doi:10.1038/nature11927 (2013).
746 13 O'Hara, B. J., Barth, Z. K., McKitterick, A. C. & Seed, K. D. A highly specific phage defense system
747 is a conserved feature of the *Vibrio cholerae* mobilome. *PLoS Genet* **13**, e1006838,
748 doi:10.1371/journal.pgen.1006838 (2017).
749 14 Angermeyer, A. *et al.* Evolutionary Sweeps of Subviral Parasites and Their Phage Host Bring
750 Unique Parasite Variants and Disappearance of a Phage CRISPR-Cas System. *mBio* **13**, e03088-
751 21, doi:10.1128/mbio.03088-21 (2022).
752 15 Seed, K. D. *et al.* Evolutionary consequences of intra-patient phage predation on microbial
753 populations. *Elife* **3**, e03497, doi:10.7554/eLife.03497 (2014).
754 16 Beckman, D. A. & Waters, C. M. *Vibrio cholerae* phage ICP3 requires O1 antigen for infection.
755 *Infect Immun* **91**, e0002623, doi:10.1128/iai.00026-23 (2023).

17 Alam, M. T. *et al.* Emergence and Evolutionary Response of *Vibrio cholerae* to Novel Bacteriophage, Democratic Republic of the Congo. *Emerg Infect Dis* **28**, 2482-90, doi:10.3201/eid2812.220572 (2022).
18 Hussain, F. A. *et al.* Rapid evolutionary turnover of mobile genetic elements drives bacterial resistance to phages. *Science* **374**, 488-92, doi:10.1126/science.abb1083 (2021).
19 Davies, B. W., Bogard, R. W., Young, T. S. & Mekalanos, J. J. Coordinated regulation of accessory genetic elements produces cyclic di-nucleotides for *V. cholerae* virulence. *Cell* **149**, 358-70, doi:10.1016/j.cell.2012.01.053 (2012).
20 Doron, S. *et al.* Systematic discovery of antiphage defense systems in the microbial pangenome. *Science* **359**, doi:10.1126/science.aar4120 (2018).
21 Severin, G. B. *et al.* Direct activation of a phospholipase by cyclic GMP-AMP in El Tor *Vibrio cholerae*. *Proc Natl Acad Sci U S A* **115**, E6048-E55, doi:10.1073/pnas.1801233115 (2018).
22 Cohen, D. *et al.* Cyclic GMP-AMP signalling protects bacteria against viral infection. *Nature* **574**, 691-95, doi:10.1038/s41586-019-1605-5 (2019).
23 Hsueh, B. Y. *et al.* Phage defence by deaminase-mediated depletion of deoxynucleotides in bacteria. *Nat Microbiol* **7**, 1210-20, doi:10.1038/s41564-022-01162-4 (2022).
24 Jaskólska, M., Adams, D. W. & Blokesch, M. Two defence systems eliminate plasmids from seventh pandemic *Vibrio cholerae*. *Nature* **604**, 323-29, doi:10.1038/s41586-022-04546-y (2022).
25 Vizzarro, G., Lemopoulos, A., Adams, D. W. & Blokesch, M. *Vibrio cholerae* pathogenicity island 2 encodes two distinct types of restriction systems. *J Bacteriol*, e0014524, doi:10.1128/jb.00145-24 (2024).
26 Gomez, J. B. & Waters, C. M. A *Vibrio cholerae* Type IV restriction system targets glucosylated 5-hydroxymethylcytosine to protect against phage infection. *J Bacteriol*, e0014324, doi:10.1128/jb.00143-24 (2024).
27 Kumate, J., Sepúlveda, J. & Gutiérrez, G. Cholera epidemiology in Latin America and perspectives for eradication. *Bulletin de l'Institut Pasteur* **96**, 217-26, doi:10.1016/S0020-2452(99)80002-5 (1998).
28 Nusrin, S. *et al.* Peruvian *Vibrio cholerae* O1 El Tor strains possess a distinct region in the *Vibrio* seventh pandemic island-II that differentiates them from the prototype seventh pandemic El Tor strains. *J Med Microbiol* **58**, 342-54, doi:10.1099/jmm.0.005397-0 (2009).
29 Garza, D. R. *et al.* Genome-wide study of the defective sucrose fermenter strain of *Vibrio cholerae* from the Latin American cholera epidemic. *PLoS One* **7**, e37283, doi:10.1371/journal.pone.0037283 (2012).
30 Domman, D. *et al.* Integrated view of *Vibrio cholerae* in the Americas. *Science* **358**, 789-93, doi:10.1126/science.aao2136 (2017).
31 Weill, F. X. *et al.* Genomic history of the seventh pandemic of cholera in Africa. *Science* **358**, 785-89, doi:10.1126/science.aad5901 (2017).
32 Lemos Rocha, L. F. *et al.* The VarA-CsrA regulatory pathway influences cell shape in *Vibrio cholerae*. *PLoS Genet* **18**, e1010143, doi:10.1371/journal.pgen.1010143 (2022).
33 Rousset, F. *et al.* Phages and their satellites encode hotspots of antiviral systems. *Cell Host Microbe* **30**, 740-53 e5, doi:10.1016/j.chom.2022.02.018 (2022).
34 Vassallo, C. N., Doering, C. R., Littlehale, M. L., Teodoro, G. I. C. & Laub, M. T. A functional selection reveals previously undetected anti-phage defence systems in the E. coli pangenome. *Nat Microbiol* **7**, 1568-79, doi:10.1038/s41564-022-01219-4 (2022).
35 Patel, P. H. & Maxwell, K. L. Prophages provide a rich source of antiphage defense systems. *Curr Opin Microbiol* **73**, 102321, doi:10.1016/j.mib.2023.102321 (2023).
36 Krishnan, A., Burroughs, A. M., Iyer, L. M. & Aravind, L. Comprehensive classification of ABC ATPases and their functional radiation in nucleoprotein dynamics and biological conflict systems. *Nucleic Acids Res* **48**, 10045-75, doi:10.1093/nar/gkaa726 (2020).
37 Steczkiewicz, K., Muszewska, A., Knizewski, L., Rychlewski, L. & Ginalski, K. Sequence, structure and functional diversity of PD-(D/E)XK phosphodiesterase superfamily. *Nucleic Acids Res* **40**, 7016-45, doi:10.1093/nar/gks382 (2012).

38 Maffei, E. *et al.* Systematic exploration of *Escherichia coli* phage-host interactions with the BASEL phage collection. *PLoS Biol* **19**, e3001424, doi:10.1371/journal.pbio.3001424 (2021).
39 Schiltz, C. J., Adams, M. C. & Chappie, J. S. The full-length structure of *Thermus scotoductus* OLD defines the ATP hydrolysis properties and catalytic mechanism of Class 1 OLD family nucleases. *Nucleic Acids Res* **48**, 2762-76, doi:10.1093/nar/gkaa059 (2020).
40 Antine, S. P. *et al.* Structural basis of Gabija anti-phage defence and viral immune evasion. *Nature* **625**, 360-65, doi:10.1038/s41586-023-06855-2 (2024).
41 Burman, N. *et al.* A virally-encoded tRNA neutralizes the PARIS antiviral defence system. *Nature*, doi:10.1038/s41586-024-07874-3 (2024).
42 Deep, A., Liang, Q., Enustun, E., Pogliano, J. & Corbett, K. D. Architecture and activation mechanism of the bacterial PARIS defence system. *Nature*, doi:10.1038/s41586-024-07772-8 (2024).
43 Li, Y. *et al.* PtuA and PtuB assemble into an inflammasome-like oligomer for anti-phage defense. *Nat Struct Mol Biol* **31**, 413-23, doi:10.1038/s41594-023-01172-8 (2024).
44 Dot, E. W., Thomason, L. C. & Chappie, J. S. Everything OLD is new again: How structural, functional, and bioinformatic advances have redefined a neglected nuclease family. *Mol Microbiol* **120**, 122-40, doi:10.1111/mmi.15074 (2023).
45 Payne, L. J., Hughes, T. C. D., Fineran, P. C. & Jackson, S. A. New antiviral defences are genetically embedded within prokaryotic immune systems. *bioRxiv*, 2024.01.29.577857, doi:10.1101/2024.01.29.577857 (2024).
46 Rousset, F. & Sorek, R. The evolutionary success of regulated cell death in bacterial immunity. *Curr Opin Microbiol* **74**, 102312, doi:10.1016/j.mib.2023.102312 (2023).
47 Seed, K. D. *et al.* Phase variable O antigen biosynthetic genes control expression of the major protective antigen and bacteriophage receptor in *Vibrio cholerae* O1. *PLoS Pathog* **8**, e1002917, doi:10.1371/journal.ppat.1002917 (2012).
48 Barth, Z. K., Netter, Z., Angermeyer, A., Bhardwaj, P. & Seed, K. D. A Family of Viral Satellites Manipulates Invading Virus Gene Expression and Can Affect Cholera Toxin Mobilization. *mSystems* **5**, doi:10.1128/mSystems.00358-20 (2020).
49 McKitterick, A. C., Hays, S. G., Johura, F. T., Alam, M. & Seed, K. D. Viral Satellites Exploit Phage Proteins to Escape Degradation of the Bacterial Host Chromosome. *Cell Host Microbe* **26**, 504-14 e4, doi:10.1016/j.chom.2019.09.006 (2019).
50 Jurenas, D., Fraikin, N., Goormaghtigh, F. & Van Melderen, L. Biology and evolution of bacterial toxin-antitoxin systems. *Nat Rev Microbiol* **20**, 335-50, doi:10.1038/s41579-021-00661-1 (2022).
51 Patel, K. M. & Seed, K. D. Sporadic phage defense in epidemic *Vibrio cholerae* mediated by the toxin-antitoxin system DarTG is countered by a phage-encoded antitoxin mimic. *mBio* **15**, e0011124, doi:10.1128/mbio.00111-24 (2024).
52 Nonejuie, P., Burkart, M., Pogliano, K. & Pogliano, J. Bacterial cytological profiling rapidly identifies the cellular pathways targeted by antibacterial molecules. *Proc Natl Acad Sci U S A* **110**, 16169-74, doi:10.1073/pnas.1311066110 (2013).
53 Murphy, S. G., Johnson, B. A., Ledoux, C. M. & Dörr, T. *Vibrio cholerae*'s mysterious Seventh Pandemic island (VSP-II) encodes novel Zur-regulated zinc starvation genes involved in chemotaxis and cell congregation. *PLoS Genet* **17**, e1009624, doi:10.1371/journal.pgen.1009624 (2021).
54 Hutinet, G. *et al.* 7-Deazaguanine modifications protect phage DNA from host restriction systems. *Nat Commun* **10**, 5442, doi:10.1038/s41467-019-13384-y (2019).
55 Hutinet, G., Lee, Y. J., de Crécy-Lagard, V. & Weigele, P. R. Hypermodified DNA in Viruses of *E. coli* and *Salmonella*. *EcoSal Plus* **9**, eESP00282019, doi:10.1128/ecosalplus.ESP-0028-2019 (2021).
56 Machnicka, M. A., Kaminska, K. H., Dunin-Horkawicz, S. & Bujnicki, J. M. Phylogenomics and sequence-structure-function relationships in the GmrSD family of Type IV restriction enzymes. *BMC Bioinformatics* **16**, 336, doi:10.1186/s12859-015-0773-z (2015).

861 57 He, X. *et al.* Expression and purification of a single-chain Type IV restriction enzyme
862 Eco94GmrSD and determination of its substrate preference. *Sci Rep* **5**, 9747,
863 doi:10.1038/srep09747 (2015).
864 58 Picton, D. M. *et al.* The phage defence island of a multidrug resistant plasmid uses both BREX
865 and type IV restriction for complementary protection from viruses. *Nucleic Acids Res* **49**,
866 11257-73, doi:10.1093/nar/gkab906 (2021).
867 59 Xiong, X. *et al.* SspABCD-SspE is a phosphorothioation-sensing bacterial defence system with
868 broad anti-phage activities. *Nat Microbiol* **5**, 917-28, doi:10.1038/s41564-020-0700-6 (2020).
869 60 Gao, H. *et al.* Nicking mechanism underlying the DNA phosphorothioate-sensing antiphage
870 defense by SspE. *Nat Commun* **13**, 6773, doi:10.1038/s41467-022-34505-0 (2022).
871 61 Jablonska, J., Matelska, D., Steczkiewicz, K. & Ginalski, K. Systematic classification of the His-
872 Me finger superfamily. *Nucleic Acids Res* **45**, 11479-94, doi:10.1093/nar/gkx924 (2017).
873 62 Gedara, S. H. *et al.* 7-Deazaguanines in DNA: functional and structural elucidation of a DNA
874 modification system. *Nucleic Acids Res* **51**, 3836-54, doi:10.1093/nar/gkad141 (2023).
875 63 Dutta, R. & Inouye, M. GHKL, an emergent ATPase/kinase superfamily. *Trends Biochem Sci* **25**,
876 24-8, doi:10.1016/s0968-0004(99)01503-0 (2000).
877 64 Iyer, L. M., Abhiman, S. & Aravind, L. MutL homologs in restriction-modification systems and
878 the origin of eukaryotic MORC ATPases. *Biol Direct* **3**, 8, doi:10.1186/1745-6150-3-8 (2008).
879 65 Gu, Y. *et al.* Bacterial Shedu immune nucleases share a common enzymatic core regulated by
880 diverse sensor domains. *Mol Cell*, doi:10.1016/j.molcel.2024.12.004 (2025).
881 66 Loeff, L., Walter, A., Rosalen, G. T. & Jinek, M. DNA end sensing and cleavage by the Shedu
882 anti-phage defense system. *Cell*, doi:10.1016/j.cell.2024.11.030 (2025).
883 67 Corbett, K. D. & Berger, J. M. Structural dissection of ATP turnover in the prototypical GHL
884 ATPase TopoVI. *Structure* **13**, 873-82, doi:10.1016/j.str.2005.03.013 (2005).
885 68 Nicolle, P., Gallut, J., Ducrest, P. & Quiniou, J. Recherches en vue d'établir une lysotypie pour
886 les vibrions cholériques et les vibrions d'El-Tor. *Rev. Hyg. Med. soc.* **10**, 91-126 (1962).
887 69 Darracq, B. *et al.* Sedentary chromosomal integrons as biobanks of bacterial anti-phage
888 defence systems. *bioRxiv*, 2024.07.02.601686, doi:10.1101/2024.07.02.601686 (2024).
889 70 Morais, L. L. *et al.* Population and genetic study of *Vibrio cholerae* from the amazon
890 environment confirms that the WASA-1 prophage is the main marker of the epidemic strain
891 that circulated in the region. *PLoS One* **8**, e81372, doi:10.1371/journal.pone.0081372 (2013).
892 71 Bhandare, S. G. *et al.* Complete Genome Sequences of *Vibrio cholerae*-Specific Bacteriophages
893 24 and X29. *Genome Announc* **5**, doi:10.1128/genomeA.01013-17 (2017).
894 72 Box, A. M., McGuffie, M. J., O'Hara, B. J. & Seed, K. D. Functional Analysis of Bacteriophage
895 Immunity through a Type I-E CRISPR-Cas System in *Vibrio cholerae* and Its Application in
896 Bacteriophage Genome Engineering. *J Bacteriol* **198**, 578-90, doi:10.1128/JB.00747-15 (2016).
897 73 Carpenter, M. R. *et al.* CRISPR-Cas and Contact-Dependent Secretion Systems Present on
898 Excisable Pathogenicity Islands with Conserved Recombination Modules. *J Bacteriol* **199**,
899 doi:10.1128/JB.00842-16 (2017).
900 74 McDonald, N. D., Regmi, A., Morreale, D. P., Borowski, J. D. & Boyd, E. F. CRISPR-Cas systems
901 are present predominantly on mobile genetic elements in *Vibrio* species. *BMC Genomics* **20**,
902 105, doi:10.1186/s12864-019-5439-1 (2019).
903 75 Tauxe, R. V., Mintz, E. D. & Quick, R. E. Epidemic cholera in the new world: translating field
904 epidemiology into new prevention strategies. *Emerg Infect Dis* **1**, 141-6,
905 doi:10.3201/eid0104.950408 (1995).
906 76 Dorman, M. J. *et al.* Genomics of the Argentinian cholera epidemic elucidate the contrasting
907 dynamics of epidemic and endemic *Vibrio cholerae*. *Nat Commun* **11**, 4918,
908 doi:10.1038/s41467-020-18647-7 (2020).
909 77 Valia, R. *et al. Vibrio cholerae* O1 epidemic variants in Angola: a retrospective study between
910 1992 and 2006. *Front Microbiol* **4**, 354, doi:10.3389/fmicb.2013.00354 (2013).
911 78 Meyer, N., Stephan, R., Cernela, N., Horlbog, J. A. & Biggel, M. Genomic characteristics of
912 clinical non-toxigenic *Vibrio cholerae* isolates in Switzerland: a cross-sectional study. *Swiss
913 Med Wkly* **154**, 3437, doi:10.57187/s.3437 (2024).

914 79 Piel, D. *et al.* Phage-host coevolution in natural populations. *Nat Microbiol* **7**, 1075-86,
915 doi:10.1038/s41564-022-01157-1 (2022).
916 80 Lim, A. N. W., Yen, M., Seed, K. D., Lazinski, D. W. & Camilli, A. A Tail Fiber Protein and a
917 Receptor-Binding Protein Mediate ICP2 Bacteriophage Interactions with *Vibrio cholerae*
918 OmpU. *J Bacteriol* **203**, e0014121, doi:10.1128/JB.00141-21 (2021).
919 81 Eberhart-Phillips, J. *et al.* An outbreak of cholera from food served on an international aircraft.
920 *Epidemiol Infect* **116**, 9-13, doi:10.1017/s0950268800058891 (1996).
921 82 Yildiz, F. H. & Schoolnik, G. K. Role of *rpoS* in stress survival and virulence of *Vibrio cholerae*. *J*
922 *Bacteriol* **180**, 773-84, doi:10.1128/JB.180.4.773-784.1998 (1998).
923 83 Matthey, N., Drebes Dörr, N. C. & Blokesch, M. Long-Read-Based Genome Sequences of
924 Pandemic and Environmental *Vibrio cholerae* Strains. *Microbiol Resour Announc* **7**,
925 doi:10.1128/MRA.01574-18 (2018).
926 84 Aoki, S. K. *et al.* A universal biomolecular integral feedback controller for robust perfect
927 adaptation. *Nature* **570**, 533-37, doi:10.1038/s41586-019-1321-1 (2019).
928 85 Simon, R., Priefer, U. & Pühler, A. A Broad Host Range Mobilization System for In Vivo Genetic
929 Engineering: Transposon Mutagenesis in Gram Negative Bacteria. *Bio/Technology* **1**, 784-91,
930 doi:10.1038/nbt1183-784 (1983).
931 86 Ferrières, L. *et al.* Silent mischief: bacteriophage Mu insertions contaminate products of
932 *Escherichia coli* random mutagenesis performed using suicidal transposon delivery plasmids
933 mobilized by broad-host-range RP4 conjugative machinery. *J Bacteriol* **192**, 6418-27,
934 doi:10.1128/JB.00621-10 (2010).
935 87 Marvig, R. L. & Blokesch, M. Natural transformation of *Vibrio cholerae* as a tool--optimizing
936 the procedure. *BMC Microbiol* **10**, 155, doi:10.1186/1471-2180-10-155 (2010).
937 88 De Souza Silva, O. & Blokesch, M. Genetic manipulation of *Vibrio cholerae* by combining
938 natural transformation with FLP recombination. *Plasmid* **64**, 186-95,
939 doi:10.1016/j.plasmid.2010.08.001 (2010).
940 89 Blokesch, M. TransFLP-a method to genetically modify *Vibrio cholerae* based on natural
941 transformation and FLP-recombination. *J Vis Exp*, doi:10.3791/3761 (2012).
942 90 Van der Henst, C. *et al.* Molecular insights into *Vibrio cholerae*'s intra-amoebal host-pathogen
943 interactions. *Nat Commun* **9**, 3460, doi:10.1038/s41467-018-05976-x (2018).
944 91 Meibom, K. L. *et al.* The *Vibrio cholerae* chitin utilization program. *Proc Natl Acad Sci U S A*
945 **101**, 2524-9, doi:10.1073/pnas.0308707101 (2004).
946 92 Bao, Y., Lies, D. P., Fu, H. & Roberts, G. P. An improved Tn7-based system for the single-copy
947 insertion of cloned genes into chromosomes of gram-negative bacteria. *Gene* **109**, 167-8,
948 doi:10.1016/0378-1119(91)90604-a (1991).
949 93 Ducret, A., Quardokus, E. M. & Brun, Y. V. MicrobeJ, a tool for high throughput bacterial cell
950 detection and quantitative analysis. *Nat Microbiol* **1**, 16077, doi:10.1038/nmicrobiol.2016.77
951 (2016).
952 94 Lo Scrudato, M. & Blokesch, M. The regulatory network of natural competence and
953 transformation of *Vibrio cholerae*. *PLoS Genet* **8**, e1002778,
954 doi:10.1371/journal.pgen.1002778 (2012).
955 95 Tesson, F. *et al.* Systematic and quantitative view of the antiviral arsenal of prokaryotes. *Nat*
956 *Commun* **13**, 2561, doi:10.1038/s41467-022-30269-9 (2022).
957 96 Payne, L. J. *et al.* PADLOC: a web server for the identification of antiviral defence systems in
958 microbial genomes. *Nucleic Acids Res* **50**, W541-W50, doi:10.1093/nar/gkac400 (2022).
959 97 Zimmermann, L. *et al.* A Completely Reimplemented MPI Bioinformatics Toolkit with a New
960 HHpred Server at its Core. *J Mol Biol* **430**, 2237-43, doi:10.1016/j.jmb.2017.12.007 (2018).
961 98 Holm, L., Laiho, A., Törönen, P. & Salgado, M. DALI shines a light on remote homologs: One
962 hundred discoveries. *Protein Sci* **32**, e4519, doi:10.1002/pro.4519 (2023).
963 99 Abramson, J. *et al.* Accurate structure prediction of biomolecular interactions with AlphaFold
964 3. *Nature* **630**, 493-500, doi:10.1038/s41586-024-07487-w (2024).
965 100 Crooks, G. E., Hon, G., Chandonia, J. M. & Brenner, S. E. WebLogo: a sequence logo generator.
966 *Genome Res* **14**, 1188-90, doi:10.1101/gr.849004 (2004).

101 Katoh, K. & Standley, D. M. MAFFT multiple sequence alignment software version 7: improvements in performance and usability. *Mol Biol Evol* **30**, 772-80, doi:10.1093/molbev/mst010 (2013).
102 Gilchrist, C. L. M. & Chooi, Y. H. clinker & clustermap.js: automatic generation of gene cluster comparison figures. *Bioinformatics* **37**, 2473-75, doi:10.1093/bioinformatics/btab007 (2021).
103 Abby, S. S., Néron, B., Ménager, H., Touchon, M. & Rocha, E. P. MacSyFinder: a program to mine genomes for molecular systems with an application to CRISPR-Cas systems. *PLoS One* **9**, e110726, doi:10.1371/journal.pone.0110726 (2014).
104 Eddy, S. R. Accelerated Profile HMM Searches. *PLoS Comput Biol* **7**, e1002195, doi:10.1371/journal.pcbi.1002195 (2011).
105 Stokar-Avihail, A. *et al.* Discovery of phage determinants that confer sensitivity to bacterial immune systems. *Cell* **186**, 1863-76 e16, doi:10.1016/j.cell.2023.02.029 (2023).
106 Wick, R. R., Judd, L. M., Gorrie, C. L. & Holt, K. E. Unicycler: Resolving bacterial genome assemblies from short and long sequencing reads. *PLoS Comput Biol* **13**, e1005595, doi:10.1371/journal.pcbi.1005595 (2017).
107 Durbin, R., De Sanctis, B. & Blumer, M. Rotate: A command-line program to rotate circular DNA sequences to start at a given position or string. *Wellcome Open Res* **8**, 401, doi:10.12688/wellcomeopenres.19568.1 (2023).
108 Page, A. J. *et al.* SNP-sites: rapid efficient extraction of SNPs from multi-FASTA alignments. *Microb Genom* **2**, e000056, doi:10.1099/mgen.0.000056 (2016).
109 Stutzmann, S. & Blokesch, M. Comparison of chitin-induced natural transformation in pandemic *Vibrio cholerae* O1 El Tor strains. *Environ Microbiol* **22**, 4149-66, doi:10.1111/1462-2920.15214 (2020).
110 Kolmogorov, M., Yuan, J., Lin, Y. & Pevzner, P. A. Assembly of long, error-prone reads using repeat graphs. *Nat Biotechnol* **37**, 540-46, doi:10.1038/s41587-019-0072-8 (2019).
111 Chattopadhyay, D. J. *et al.* New phage typing scheme for *Vibrio cholerae* O1 biotype El Tor strains. *J Clin Microbiol* **31**, 1579-85, doi:10.1128/jcm.31.6.1579-1585.1993 (1993).
112 Drebes Dörr, N. C., Lemopoulos, A. & Blokesch, M. Exploring Mobile Genetic Elements in *Vibrio cholerae*. *bioRxiv*, 2024.07.25.605194, doi:10.1101/2024.07.25.605194 (2024).
113 Heidelberg, J. F. *et al.* DNA sequence of both chromosomes of the cholera pathogen *Vibrio cholerae*. *Nature* **406**, 477-83, doi:10.1038/35020000 (2000).
114 Pearson, G. D., Woods, A., Chiang, S. L. & Mekalanos, J. J. CTX genetic element encodes a site-specific recombination system and an intestinal colonization factor. *Proc Natl Acad Sci U S A* **90**, 3750-4, doi:10.1073/pnas.90.8.3750 (1993).
115 Miller, V. L., DiRita, V. J. & Mekalanos, J. J. Identification of *toxS*, a regulatory gene whose product enhances *toxR*-mediated activation of the cholera toxin promoter. *J Bacteriol* **171**, 1288-93, doi:10.1128/jb.171.3.1288-1293.1989 (1989).
116 Wachsmuth, I. K. *et al.* The molecular epidemiology of cholera in Latin America. *J Infect Dis* **167**, 621-6, doi:10.1093/infdis/167.3.621 (1993).
117 Blokesch, M. & Schoolnik, G. K. Serogroup conversion of *Vibrio cholerae* in aquatic reservoirs. *PLoS Pathog* **3**, e81, doi:10.1371/journal.ppat.0030081 (2007).
118 Metzger, L. C. *et al.* Independent Regulation of Type VI Secretion in *Vibrio cholerae* by TfoX and TfoY. *Cell Rep* **15**, 951-58, doi:10.1016/j.celrep.2016.03.092 (2016).
119 Adams, D. W., Stutzmann, S., Stoudmann, C. & Blokesch, M. DNA-uptake pili of *Vibrio cholerae* are required for chitin colonization and capable of kin recognition via sequence-specific self-interaction. *Nat Microbiol* **4**, 1545-57, doi:10.1038/s41564-019-0479-5 (2019).
120 Angermeyer, A., Das, M. M., Singh, D. V. & Seed, K. D. Analysis of 19 Highly Conserved *Vibrio cholerae* Bacteriophages Isolated from Environmental and Patient Sources Over a Twelve-Year Period. *Viruses* **10**, doi:10.3390/v10060299 (2018).
121 O'Hara, B. J., Alam, M. & Ng, W. L. The *Vibrio cholerae* Seventh Pandemic Islands act in tandem to defend against a circulating phage. *PLoS Genet* **18**, e1010250, doi:10.1371/journal.pgen.1010250 (2022).

1020 **Acknowledgments**

1021 We thank all the members of the Blokesch laboratory for constructive feedback throughout the
1022 project. We also gratefully acknowledge K. D. Seed (University of California, Berkeley), A. Camilli (Tufts
1023 University School of Medicine, Boston), W.-L. Ng (Tufts University School of Medicine, Boston) and A.
1024 Ali (University of Florida, Gainesville) for sharing ICP phages, and A. Harms (ETH, Zurich) for sharing
1025 the BASEL collection. We thank the Félix d'Hérelle Reference Center for Bacterial Viruses from the
1026 Université Laval (Québec, Canada) for providing phage X29 (HER66). Finally, we acknowledge Roger
1027 Stephan and Michael Biggel (University of Zurich) for sharing *V. cholerae* isolates from Switzerland and
1028 for valuable scientific discussions.

1029

1030 **Funding**

1031 European Research Council Consolidator Grant 724630 (MB)

1032 Swiss National Research Foundation 310030_185022 (MB)

1033 HHMI International Scholarship 55008726 (MB)

1034 EPFL intramural funding (MB)

1035

1036 **Author contributions**

1037 Conceptualization: DWA, MJ and MB

1038 Methodology: DWA, MJ, AL, and MB

1039 Investigation: DWA, MJ, AL, SS, LR, LB and MB

1040 Visualization: DWA

1041 Funding acquisition: MB

1042 Supervision: DWA and MB

1043 Writing – original draft: DWA

1044 Writing – review & editing: DWA, MJ and MB

1045 Writing – revision: DWA and MB

1046

Competing interests

Authors declare that they have no competing interests.

Supplementary information

Diverse phage defence systems define West African South American pandemic *Vibrio cholerae*

David W. Adams[1,2]*, Milena Jaskólska[1], Alexandre Lemopoulos[1], Sandrine Stutzmann[1], Laurie Righi[1], Loriane Bader[1] and Melanie Blokesch[1,2]*

[1]Laboratory of Molecular Microbiology, Global Health Institute, School of Life Sciences, Station 19, EPFL-SV-UPBLO, Ecole Polytechnique Fédérale de Lausanne (EPFL), CH-1015 Lausanne, Switzerland.

[2]These authors contributed equally

*Corresponding authors: david.adams@epfl.ch and melanie.blokesch@epfl.ch

Contents:

Extended Data Figs. 1 to 13
Captions for Tables 1 to 7
Captions for Movies 1 to 2
Caption for Supplementary Fig. 1

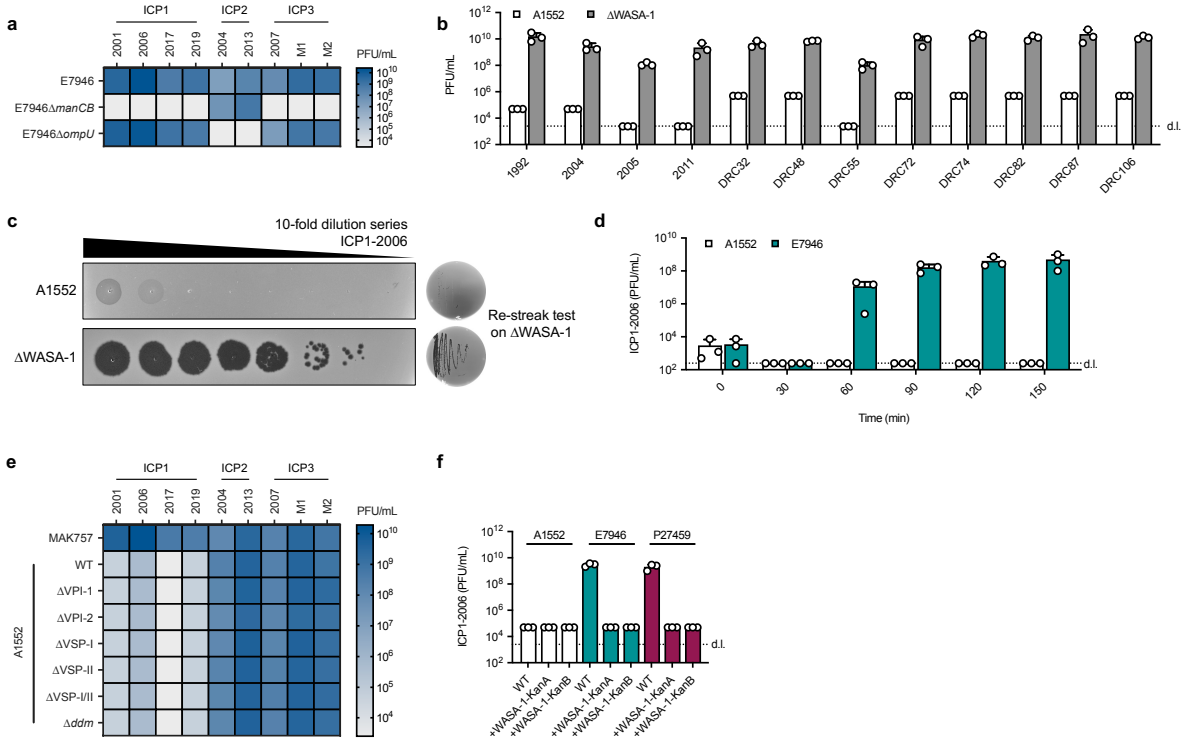

Extended Data Fig. 1. Control experiments showing role of WASA-1 prophage in ICP1 defence. (**a**) Heat-map showing mean plaque-forming units (PFU/mL) of diverse ICP1-3 isolates determined by plaque assays on E7946 derivatives that lack either the O1 antigen receptor for ICP1 and ICP3 (E7946Δ*manCB*) or the OmpU receptor for ICP2 (E7946Δ*ompU*). (**b**) Plaque assay showing PFU/mL of various ICP1 isolates on A1552 in the presence and absence of WASA-1. (**c**) Re-streak tests evaluating the propagation of viable ICP1 phage progeny were conducted by taking material from the highest concentration spot of 10-fold serial dilution plaque assays done in the presence (A1552) and absence (ΔWASA-1) of WASA-1 (left) and re-streaking on fresh lawns of the susceptible ΔWASA-1 strain (right). (**d**) Replication assay showing change in PFU/mL over time following the infection of A1552 and E7946 cultures with *c.a.* 10^3-10^4 PFU of ICP1-2006. (**e**) Heat-map showing mean plaque-forming units (PFU/mL) of diverse ICP1-3 isolates determined by plaque assays on A1552 derivatives that lack the indicated genomic islands, as compared to the pre-7th pandemic control strain MAK757. (**f**) Plaque assay showing the effects of introducing WASA-1, using versions with a kanamycin resistance cassette inserted at two different positions, into the non-WASA lineage strains E7946 and P27459 on ICP1-2006 PFU/mL, as compared to the equivalent A1552 control strains. Heat-maps and bar charts show the mean from 3 independent repeats. Error bars show s.d. and d.l. = detection limit.

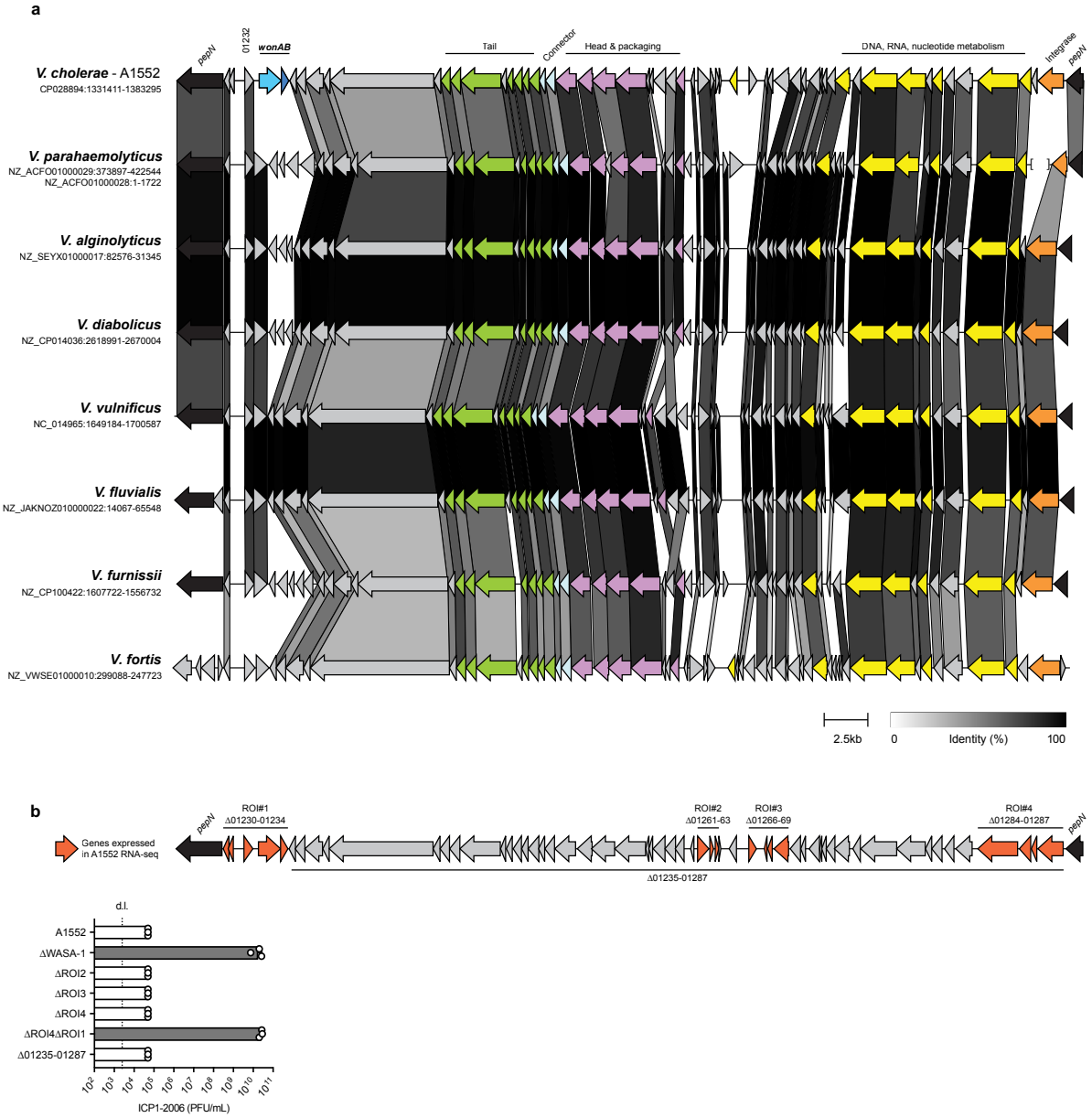

Extended Data Fig. 2. Conservation of the WASA-1 genome and identification of regions of interest. (**a**) Schematic comparing the genome organisation of WASA-1 from *V. cholerae* strain A1552 with a representative set of examples of the WASA-1 detected by BLAST in diverse *Vibrio spp*. The schematic was built using the clinker pipeline and the connections between genomes are coloured according to protein identity (above the minimum default threshold of 30%). Genes with predicted functions in prophage biology are coloured according to function, as indicated. For details of WASA-1 identification and a full list of identified sequences, see methods and Supplementary Table 2. (**b**) Schematic of *V. cholerae* strain A1552 WASA-1 highlighting the genes that were highly expressed under standard growth conditions in RNA-seq results, and which were used to define the indicated regions of interest (ROI) 1-4. Note that ROI1 could only be deleted in the ΔROI4 background. The bar chart shows the effects of deleting each ROI on ICP1-2006 PFU/mL, as compared to WT and ΔWASA-1 control strains. Bars show the mean + s.d. from 3 independent repeats. d.l. = detection limit.

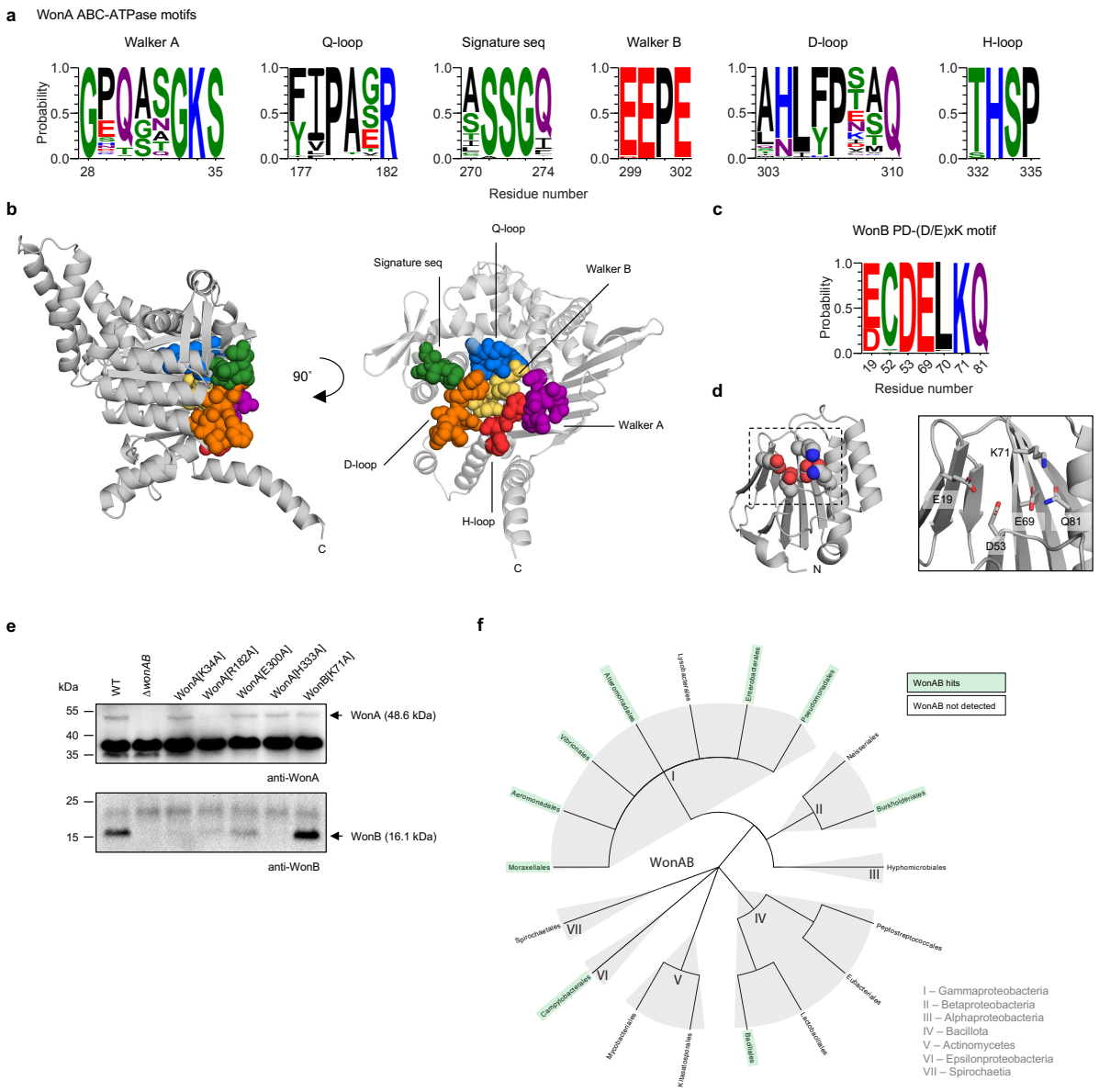

Extended Data Fig. 3. Identification of conserved motifs and distribution of WonAB. (**a**) Sequence logos showing conservation of the identified ABC-ATPase motifs in the 198 WonA hits detected using MacSyFinder v.2.1.1, as compared to the equivalent residue number in *V. cholerae* A1552 WonA. Amino acids in logos are coloured according to chemical properties: polar (G, S, T, Y, C), green; neutral (Q, N), purple; basic (K, R, H), blue; acidic (D, E), red; and hydrophobic (A, V, L, I, P, W, F, M), black. (**b**) Location of the conserved ABC-ATPase motifs shown in (**a**) at the dimer interface of the WonA dimer structural prediction. (**c**) Sequence logo showing the conservation of the identified PD-(D/E)xK nuclease motif in the 198 WonB hits detected using MacSyFinder v.2.1.1, compared to the equivalent residue number in *V. cholerae* A1552 WonB. (**d**) Location of the identified PD-(D/E)xK nuclease residues in the WonB structural prediction. (**e**) Western blot showing the protein levels of WonA and WonB, natively expressed in strain A1552 (WT) and in derivatives encoding the indicated site-directed variants. (**f**) Distribution of WonAB hits detected using MacSyFinder v.2.1.1. The tree shows the order-level phylogeny of genera in the RefSeq database with more than 500 genomes (see methods). For the full list of 198 WonAB hits see Supplementary Table 3.

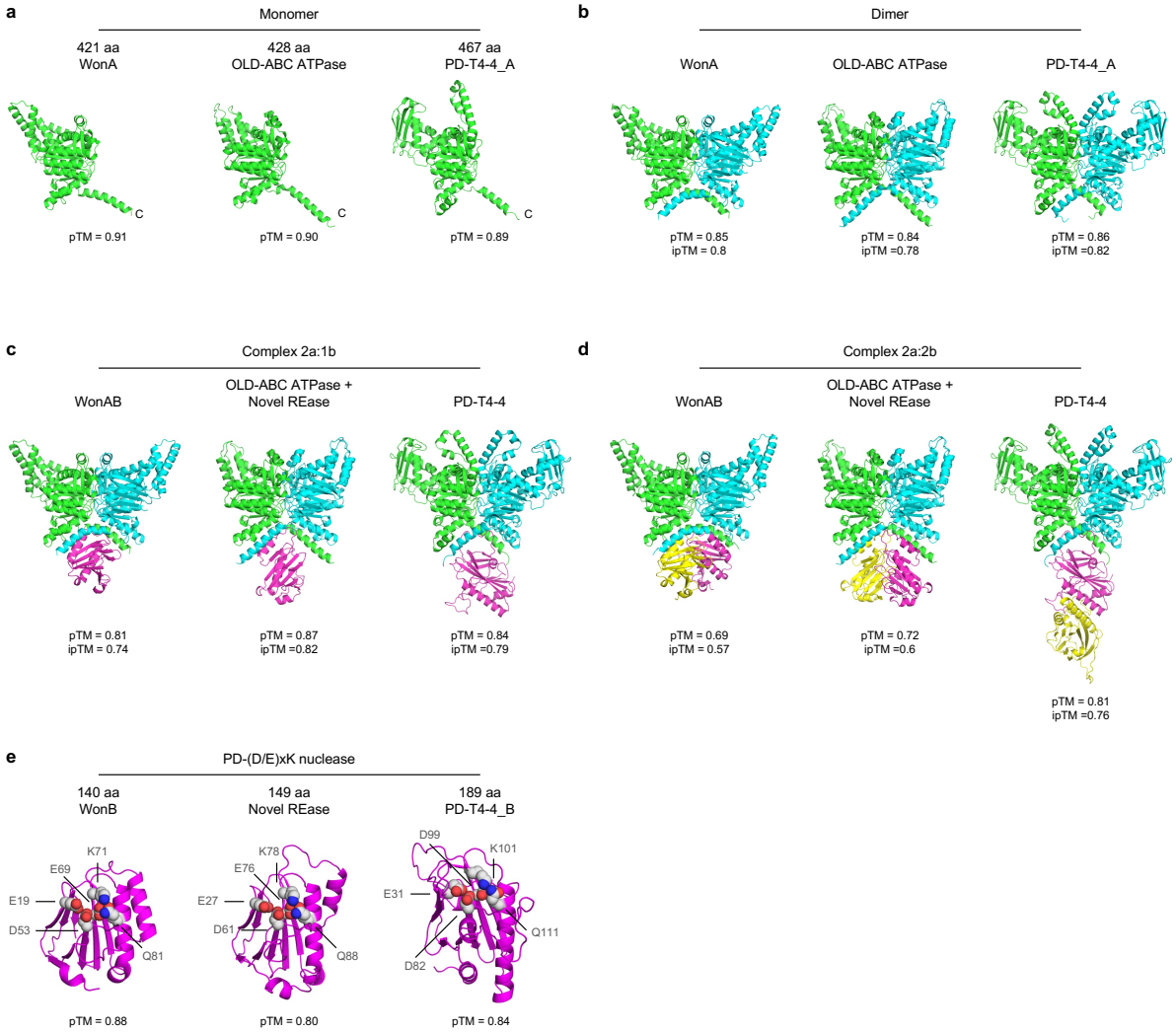

Extended Data Fig. 4. Summary of structural modelling of WonAB and related systems. (**a-e**) Cartoon representations coloured by chain showing the AlphaFold3 predicted structures for WonAB, and the related OLD-ABC ATPase + Novel REase and PD-T4-4 systems. The ATPase components WonA, OLD-ABC ATPase and PD-T4-4_A were modelled as a monomer (**a**) and a dimer (**b**), and further modelled as a complex with either one (**c**) or two (**d**) copies of the nuclease components WonB, Novel REase and PD-T4-4_B. (**e**) Nuclease components modelled alone, highlighting the location of the predicted PD-(D/E)xK nuclease residues. The predicted template modelling (pTM) score, and where appropriate, the interface predicted template modelling (ipTM) score, are shown alongside each model. Protein sequences were obtained from NCBI: *V. cholerae* A1552 WonA (AWB73975.1) and WonB (AWB73976.1); *Anaerovibrio lipolyticus* DSM 3074 OLD-ABC ATPase (SHI83489.1) + Novel REase (SHI83462.1); *E. coli* MOD1-ECOR58 PD-T4-4_A (RCO57999.1) and PD-T4-4_B (RCO57988.1).

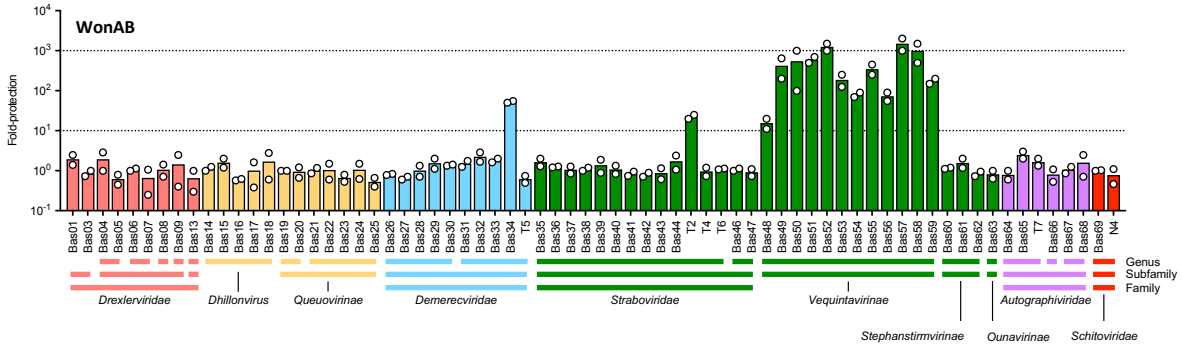

Extended Data Fig. 5. Anti-phage activity of WonAB in *E. coli*. Fold-protection against *E. coli* phages of the BASEL collection conferred by the production of WonAB in *E. coli* MG1655Δ*araCBAD*, as compared to a negative 'no system' control. The system was expressed from a chromosomally integrated transposon carrying the arabinose-inducible P_{BAD}- promoter, induced by the addition of 0.2% arabinose. Bar chart shows the mean of two independent experiments.

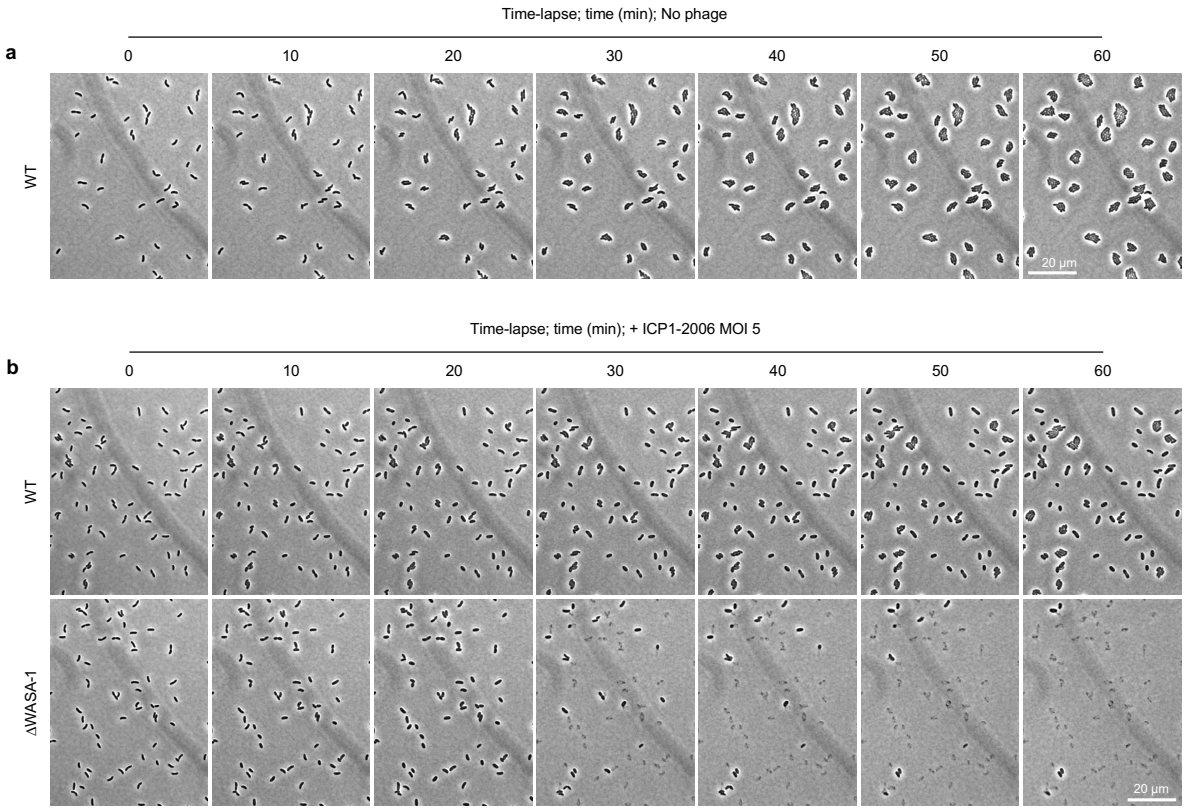

1117
1118
1119 **Extended Data Fig. 6. Time-lapse microscopy of ICP1 infection.** (**a**) Control experiment showing time-
1120 lapse microscopy of exponentially growing cells of *V. cholerae* A1552 (WT) in the absence of phage
1121 infection. (**b**) Time-lapse microscopy comparing exponentially growing cells of *V. cholerae* WT and
1122 ΔWASA-1 strains after infection with ICP1-2006 at MOI 5. The panels depict the full-frame versions of
1123 the examples presented in Fig. 2b. All images are representative of the results of three independent
1124 experiments. Scale bars = 20 µm.

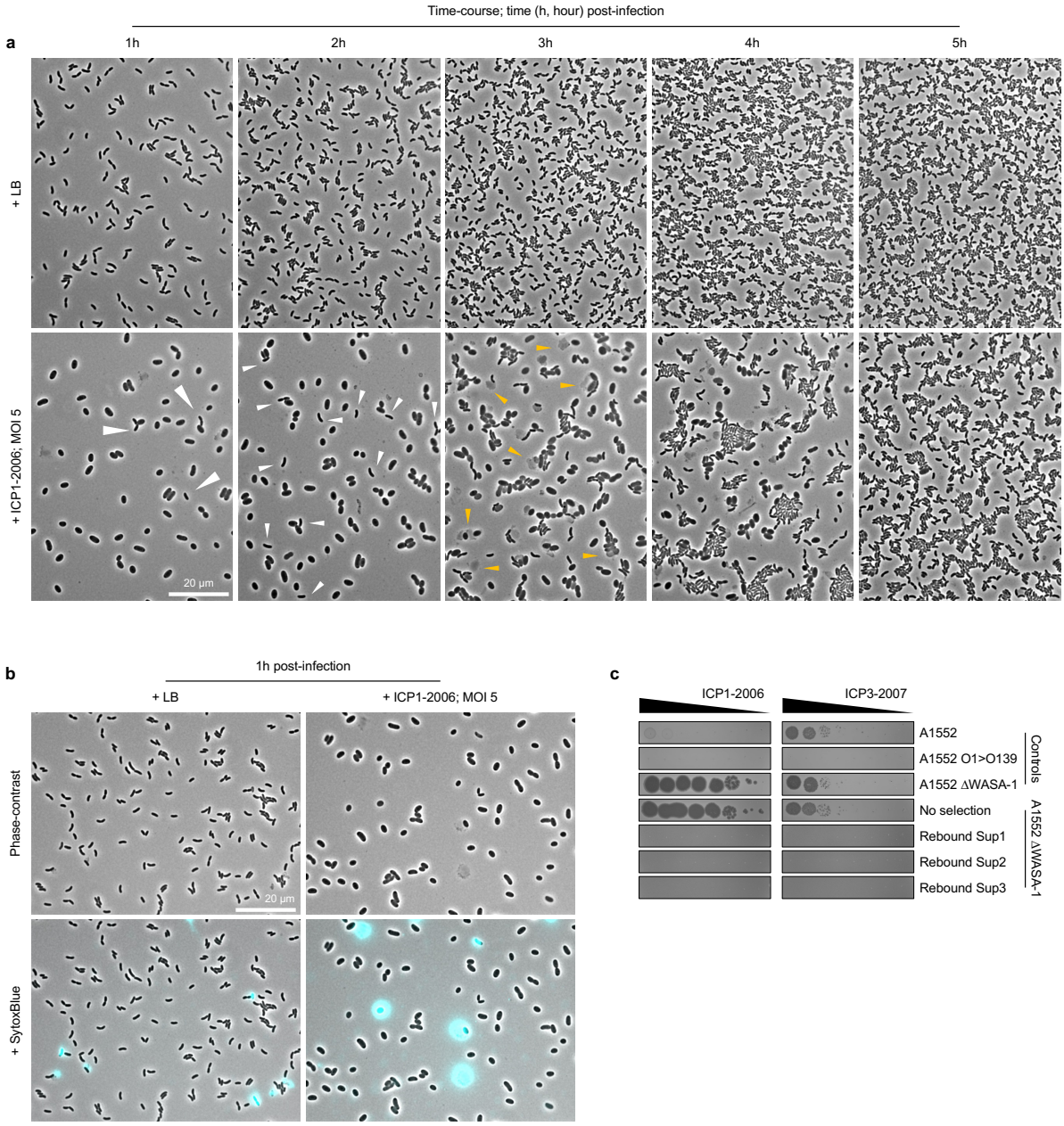

Extended Data Fig. 7. Imaging the fate of ICP1 infected cells. (**a**) Time-course microscopy snapshots comparing the growth and cell morphology of *V. cholerae* A1552 cultures at 1, 2, 3, 4 and 5 hours after infection with ICP1-2006 at MOI 5, as compared to an uninfected control culture (+ LB). Note how the ICP1-infected culture initially contains only a few cells with normal morphology (white arrowheads), and that these cells increase in number as the culture rebounds, while the swollen ICP1-infected cells that are initially dominant persist for several hours before undergoing lysis (yellow arrowheads). (**b**) SytoxBlue-staining of *V. cholerae* A1552 cultures 1 hour after infection with ICP1-2006 at MOI 5, as compared to an uninfected control culture (+ LB). (**c**) Plaque assays testing the ability of ICP1-2006 and ICP3-2007 (which both require the O1 antigen receptor) to form plaques on cultures of A1552ΔWASA-1 that rebounded following ICP1-infection, as compared to a culture of the same strain that was grown without selection, and the set of indicated control strains. Note how neither ICP1-2006 nor ICP3-2007 are able to form plaques on the rebounded cultures, consistent with recovery of the culture being driven by the growth of spontaneous O1-antigen mutant cells. All images are representative of the results of three independent experiments. Scale bars = 20 µm.

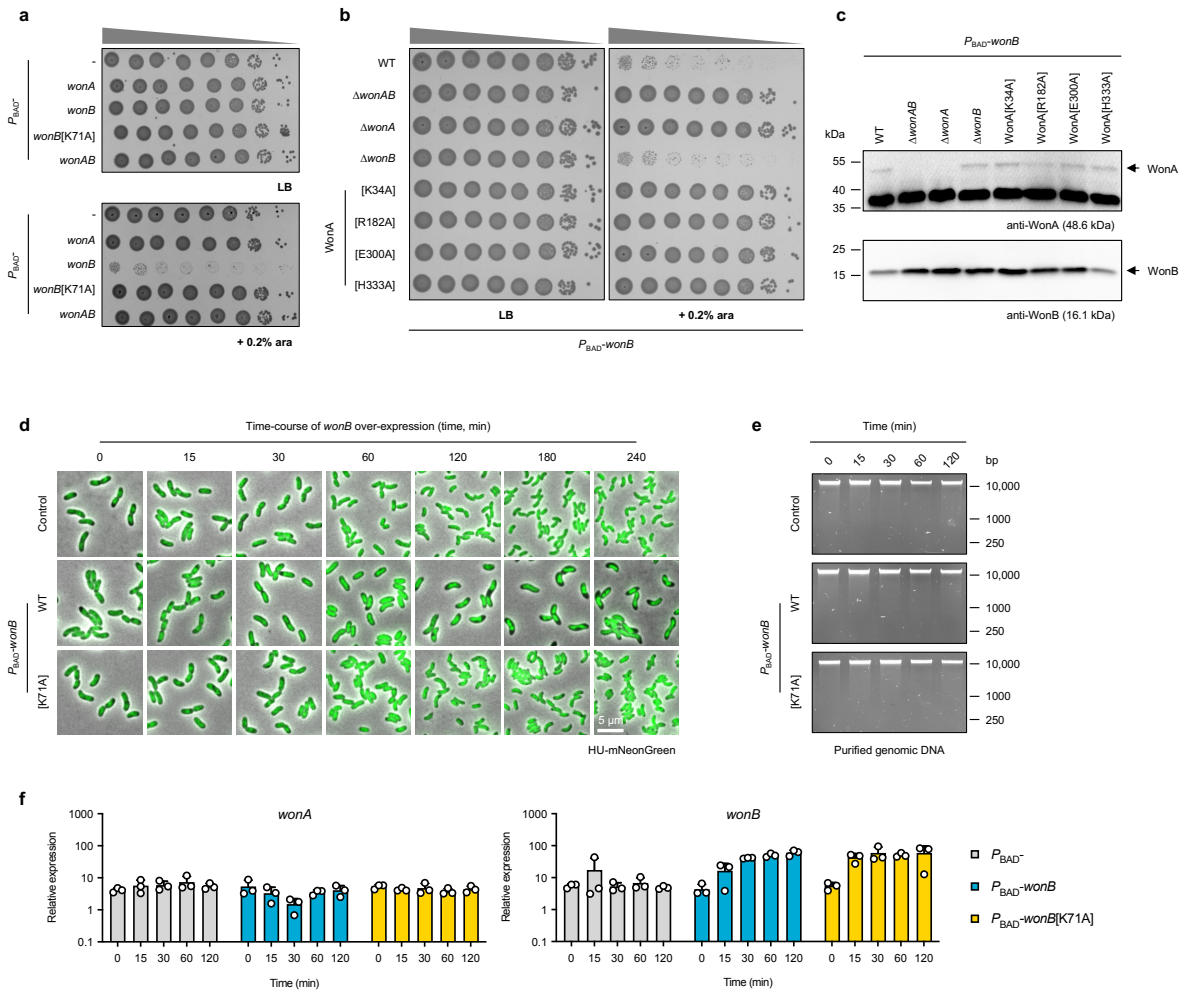

Extended Data Fig. 8. Control experiments showing details of toxicity during WonB overproduction. (**a**) Toxicity assay evaluating the growth of 10-fold serial dilutions of cultures of *V. cholerae* strain A1552 derivatives with a chromosomally integrated transposon carrying the indicated genes under the control of the arabinose-inducible P_{BAD}- promoter, in the absence (LB) and presence of induction (+ 0.2% ara), as compared to a negative control strain. (**b**) Toxicity assay evaluating the growth of 10-fold serial dilutions of *V. cholerae* strain A1552 and the indicated derivatives encoding site-directed variants of WonA, compared to the indicated deletion control strains, in the absence (LB) and presence (+ 0.2% ara) of WonB overproduction. Note that the control strains are also shown separately in Fig. 3a. (**c**) Western blots showing the protein levels of WonA and WonB in the strains used for the toxicity assay shown in (**b**). Samples were taken from exponentially growing cultures, 15 minutes after induction of P_{BAD}-*wonB*. (**d**) Time-course microscopy snapshots showing the effect of WonB overproduction on cell morphology and cellular DNA content, as monitored by a HupA-mNeonGreen fusion, compared to a negative control strain and a strain overproducing the inactive WonB[K71A] variant. Scale bar = 5 µm. The panels depict the full time-series for the examples presented in Fig. 3d. (**e**-**f**) Agarose gels evaluating the integrity of genomic DNA extractions (**e**) and comparison of *wonA* and *wonB* transcript levels as determined by qRT-PCR (**f**), prepared from cultures over time upon WonB overproduction following induction in exponentially growing cells at time 0, as compared to a negative control strain and a strain overproducing the inactive WonB[K71A] variant. All data are representative of the results of three independent repats. Bar charts show the mean + s.d.

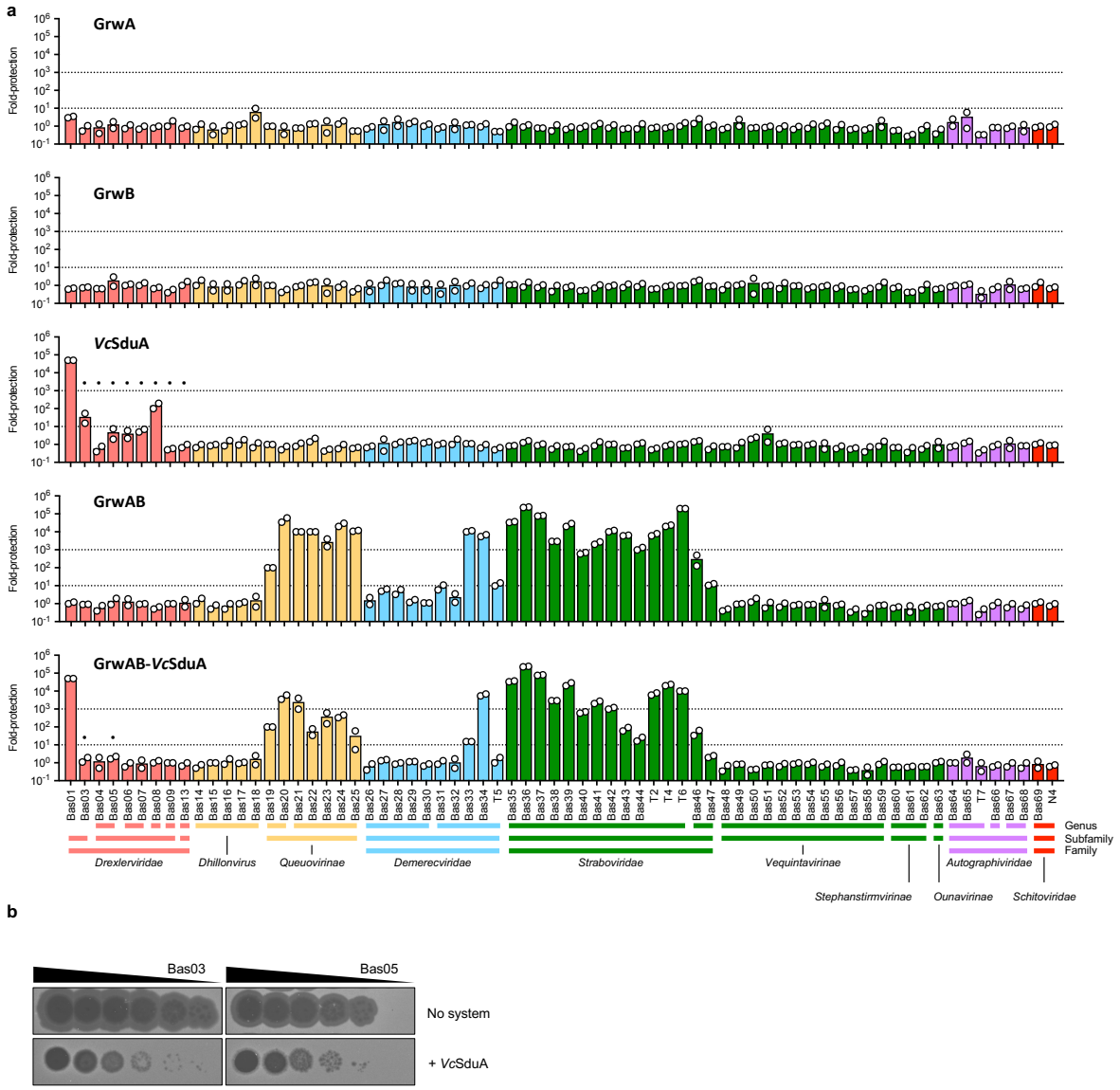

Extended Data Fig. 9. Anti-phage activity of GrwAB and *Vc*SduA in *E. coli*. (**a**) Fold-protection against *E. coli* phages of the BASEL collection conferred by the production of either GrwA, GrwB, *Vc*SduA, GrwAB or GrwAB-*Vc*SduA in *E. coli* MG1655Δ*araCBAD*, as compared to a negative 'no system' control. Genes were expressed from a chromosomally integrated transposon carrying the arabinose-inducible P_{BAD}- promoter, induced by the addition of 0.2% arabinose. Bar charts show the mean of two independent experiments. Bars with a black dot indicate phages exhibiting altered plaque morphology. (**b**) Representative examples of the altered plaque morphology phenotype observed for Bas03 and Bas05 in the presence of *Vc*SduA production.

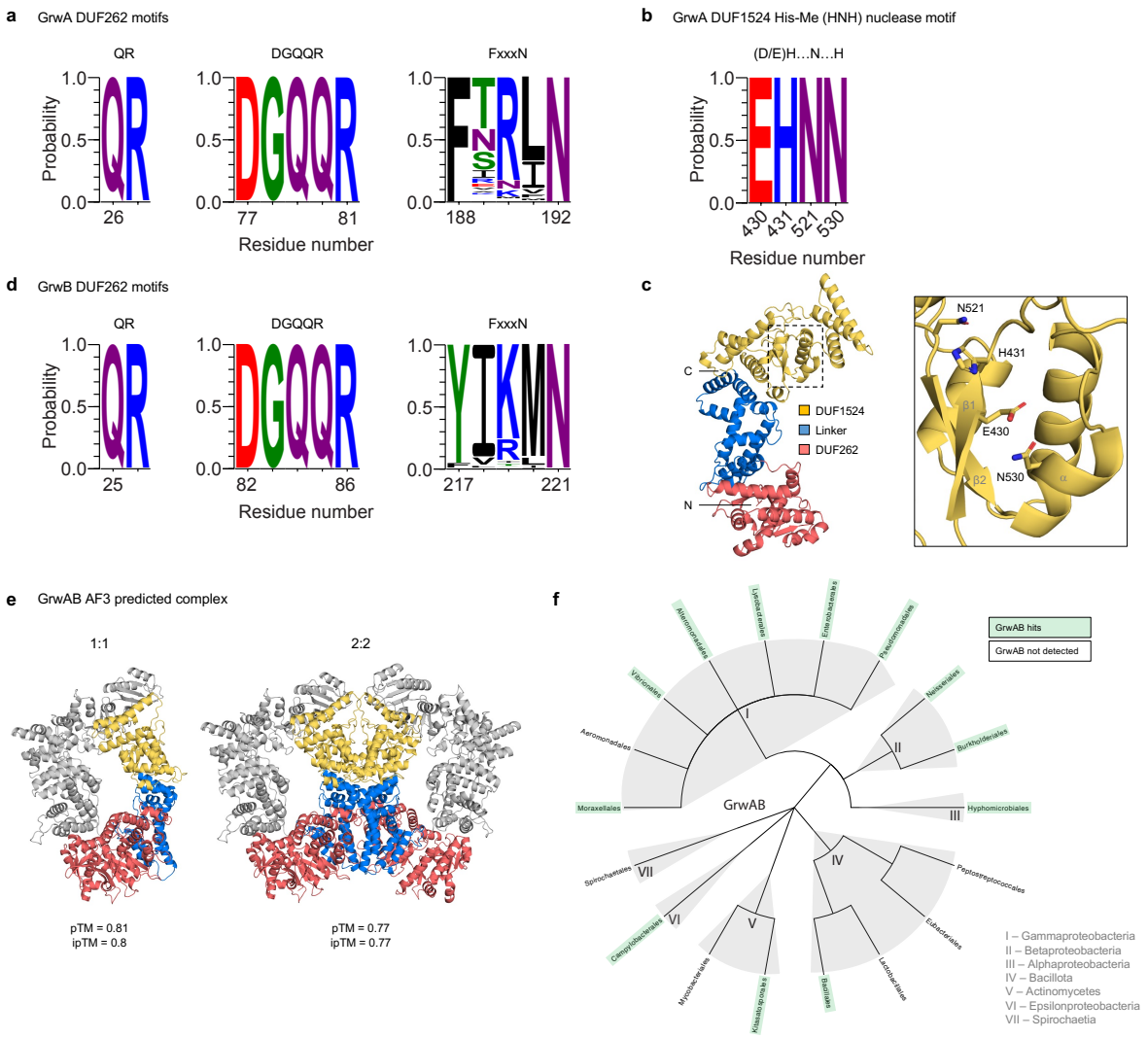

Extended Data Fig. 10. Identification of conserved motifs and distribution of GrwAB. (**a**, **d**) Sequence logos showing conservation of the identified QR, DGQQR and FxxxN motifs in the DUF262 domains of the 471 GrwA (**a**) and 471 GrwB (**d**) hits detected using MacSyFinder v.2.1.1, as compared to the equivalent residue number in *V. cholerae* A1552 GrwA and GrwB. Amino acids in logos are coloured according to chemical properties: polar (G, S, T, Y, C), green; neutral (Q, N), purple; basic (K, R, H), blue; acidic (D, E), red; and hydrophobic (A, V, L, I, P, W, F, M), black. (**b**) Sequence logo showing the conservation of the identified His-Me (HNH) nuclease motif in the DUF1524 domain of the 471 GrwA hits detected using MacSyFinder v.2.1.1, as compared to the equivalent residue number in *V. cholerae* A1552 GrwA. (**c**) Location of the identified His-Me (HNH) nuclease motif residues in the GrwA structural prediction, highlighting the predicted ββα fold. (**e**) AlphaFold3 predicted structures of potential GrwAB complexes. Colour scheme as in (**c**). (**f**) Distribution of GrwAB hits detected using MacSyFinder v.2.1.1. The tree shows the order-level phylogeny of genera in the RefSeq database with more than 500 genomes (see methods). For the full list of 471 GrwAB hits see Supplementary Table 4.

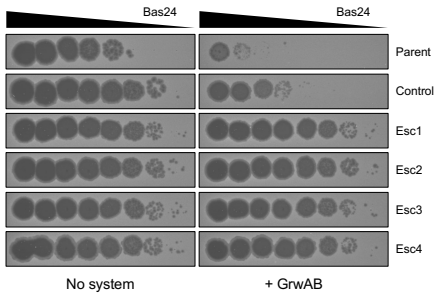

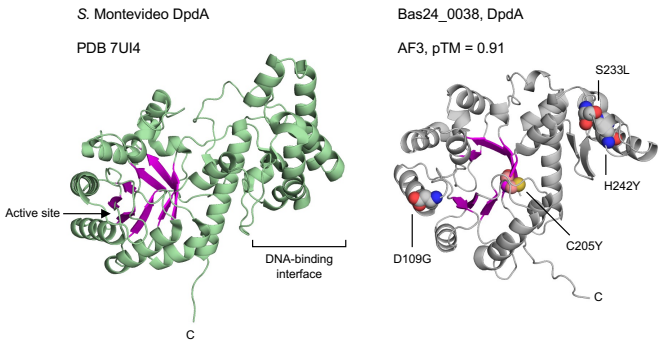

b

Bas24 *Escherichia* phage SeppeHuegi

SNP Table (0 = Absent; 1 = Present)

bp	Ref	Alt	Control	Esc1	Esc2	Esc3	Esc4	Locus	Product	Result
14,340	C	T	1	0	0	0	0	bas24_0018	HP	S61L
14,418	A	G	0	0	1	0	0	bas24_0018	HP	E87G
29,047	G	A	0	0	0	1	0	bas24_0038	DpdA	H242Y
29,073	G	A	0	0	1	0	0	bas24_0038	DpdA	S233L
29,157	C	T	0	1	0	0	0	bas24_0038	DpdA	C205Y
29,445	T	C	0	0	0	0	1	bas24_0038	DpdA	D109G
32,762	C	G	0	1	0	0	0	bas24_0044	QueC	synonymous
34,251	T	G	0	0	0	0	1	bas24_0047	QueE	intergenic, promoter region
49,229	T	C	1	0	0	0	0	bas24_0068	HP	I136V
57,705	T	C	0	1	0	0	0	bas24_0090	Nuclease	synonymous

c

Queuovirinae DpdA (7-deazaguanosine inserting enzyme) homologues

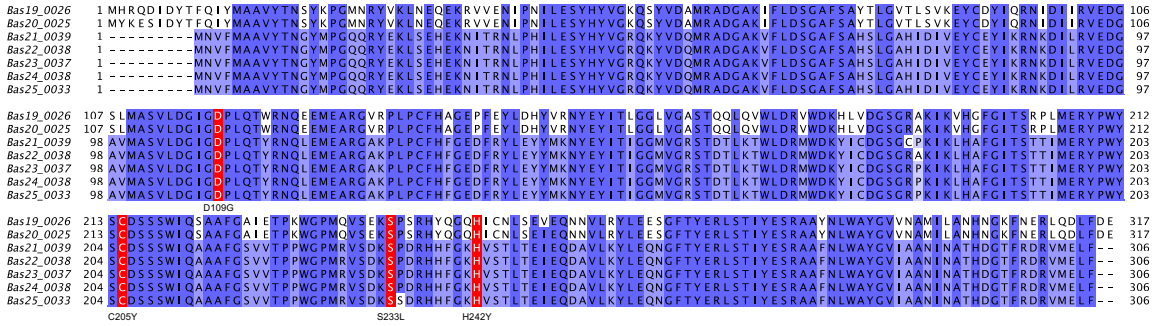

Extended Data Fig. 11. Bas24 escaper phages overcome GrwAB defence via mutations in the DNA modification pathway. (**a**) Plaque assays evaluating the ability of 10-fold serial dilutions of Bas24 escaper phages to form plaques on *E. coli* MG1655Δ*araCBAD* in the absence (No system) and presence of GrwAB (+ GrwAB), as compared to the parental Bas24 stock and a control stock propagated in the absence of GrwAB. (**b**) SNP table summarising results of whole genome sequencing for each phage compared to the published Bas24 reference sequence. Light yellow (SNP), dark yellow (SNP targeting *dpdA* locus), HP (hypothetical protein). (**c**) Multiple-sequence alignment showing conservation of *Queuovirinae* (Bas19-25) homologues of the 7-deazaguanosine inserting enzyme DpdA, with the residues found to be substituted in the Bas24 escaper phages highlighted in red. (**d**) Locations of the substituted residues shown on predicted structure of Bas24 DpdA, generated using AlphaFold3, compared to the experimentally determined crystal structure of *Salmonella enterica* serovar Montevideo DpdA (PDB 7UI4) showing the active site highlighted in magenta.

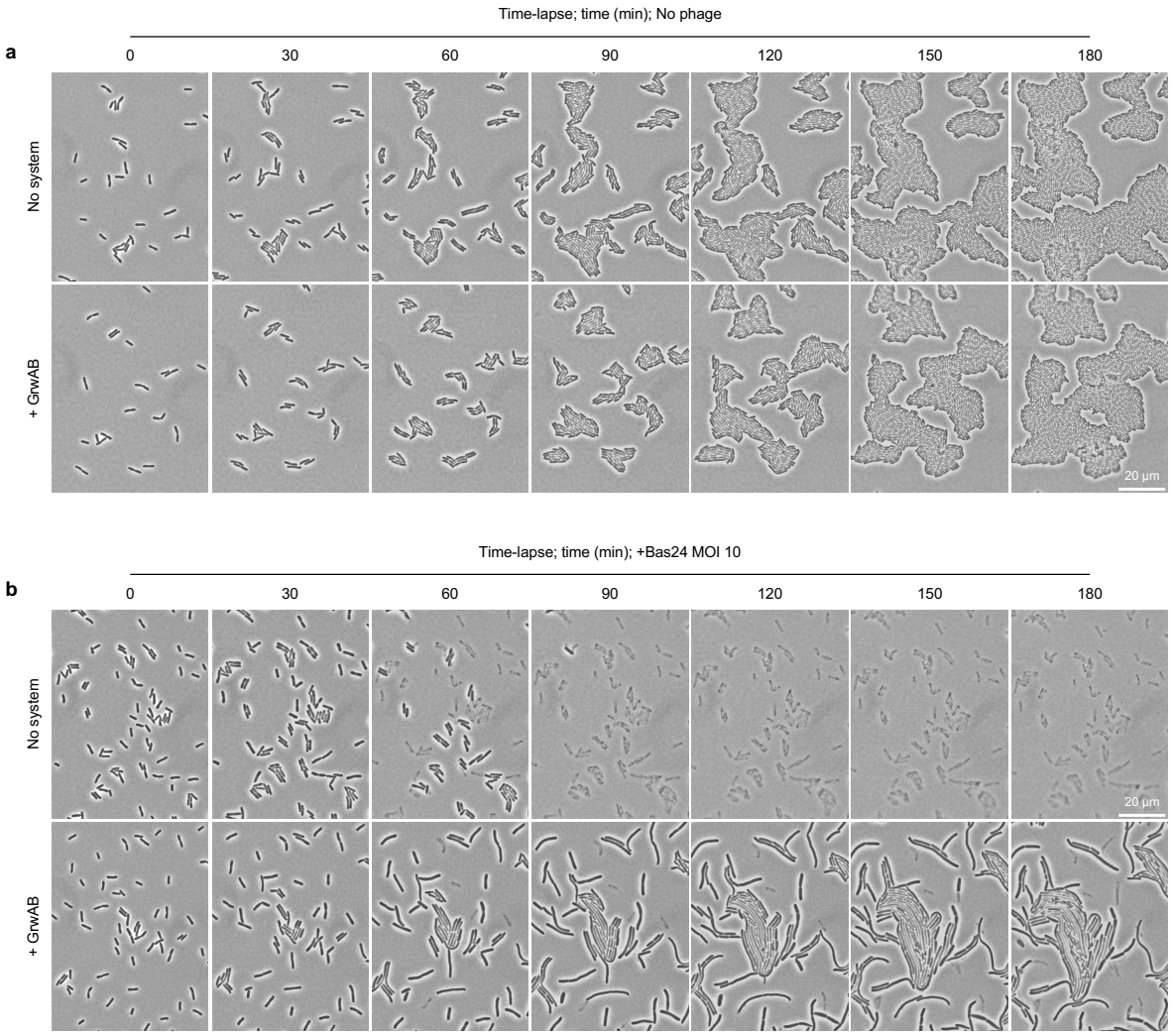

Extended Data Fig. 12. Time-lapse microscopy of Bas24 infection. (**a**-**b**) Time-lapse microscopy of exponentially growing cells of *E. coli* MG1655Δ*araCBAD* in the absence (No system) and presence (+ GrwAB) of GrwAB production, in the absence (**a**) and presence (**b**) of infection with Bas24 at MOI 10. All images are representative of the results of three independent experiments. Scale bars = 20 µm.

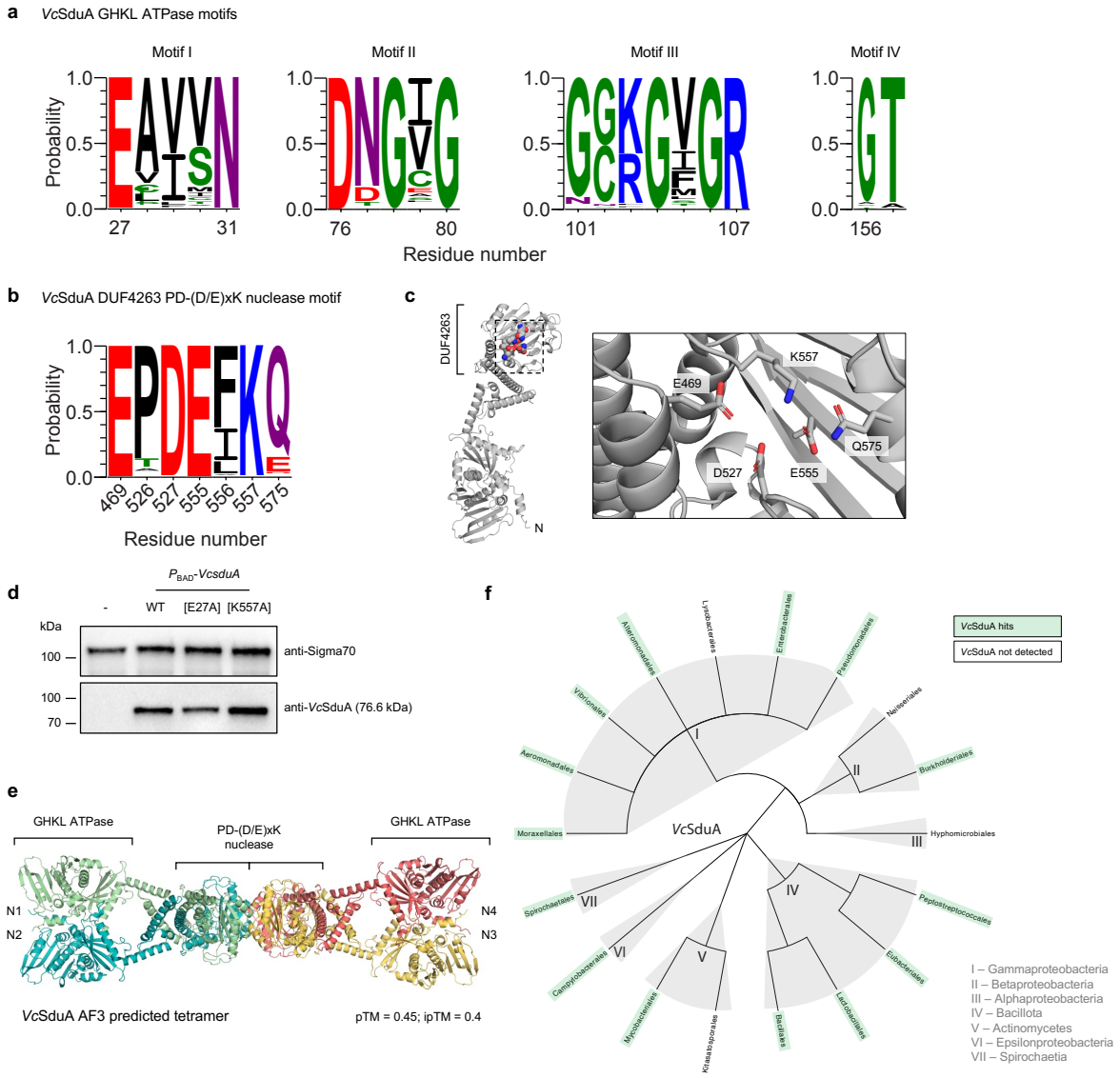

Extended Data Fig. 13. Identification of conserved motifs and distribution of *Vc*SduA. (**a**-**b**) Sequence logos showing conservation of the identified GHKL ATPase motifs I-IV in the GHKL domain (**a**) and the identified PD-(D/E)xK nuclease motif in the DUF4263 domain (**b**) of the 543 *Vc*SduA hits detected using MacSyFinder v.2.1.1, as compared to the equivalent residue number in *V. cholerae* A1552 *Vc*SduA. Amino acids in logos are coloured according to chemical properties: polar (G, S, T, Y, C), green; neutral (Q, N), purple; basic (K, R, H), blue; acidic (D, E), red; and hydrophobic (A, V, L, I, P, W, F, M), black. (**c**) Location of the identified PD-(D/E)xK nuclease residues in the *Vc*SduA structural prediction. (**d**) Western blot showing the protein levels of *Vc*SduA, expressed in *E. coli* MG1655Δ*araCBAD* from a chromosomally integrated transposon carrying the arabinose-inducible P_{BAD}- promoter, induced by the addition of 0.2% arabinose, as compared to derivatives encoding the indicated site-directed variants. Sigma70 was used as a loading control. (**e**) AlphaFold3 predicted structure of potential *Vc*SduA tetramer. (**f**) Distribution of *Vc*SduA hits detected using MacSyFinder v.2.1.1. The tree shows the order-level phylogeny of genera in the RefSeq database with more than 500 genomes (see methods). For the full list of 543 *Vc*SduA hits see Supplementary Table 5.

1223 **Supplementary Tables**

1224 **Table 1**. Summary of defence systems identified by DefenseFinder and PADLOC.

1225

1226 **Table 2**. Summary of WASA-1 hits detected by BLAST.

1227

1228 **Table 3**. Summary of matching hits for the *Vibrio cholerae* WonAB and *Anaerovibrio lipolyticus* OLD-

1229 ABC ATPase + Novel REase models, detected by MacSyFinder v.2.1.1.

1230

1231 **Table 4**. Summary of matching hits for the *Vibrio cholerae* GrwAB model detected by MacSyFinder

1232 v.2.1.1.

1233

1234 **Table 5**. Summary of matching hits for the *Vibrio cholerae Vc*SduA model detected by MacSyFinder

1235 v.2.1.1.

1236

1237 **Table 6**. Summary of DdpA-encoding vibriophages detected by BLAST.

1238

1239 **Table 7**. Bacterial strains, plasmids, bacteriophages and defence systems used in this work.

1240 **Supplementary Movies**

1241 **Movie 1**. Time-lapse microscopy of ICP1 infection.

1242 Time-lapse microscopy comparing exponentially growing cells of *V. cholerae* A1552 WT and ΔWASA-

1243 1 strains after infection with ICP1-2006 at MOI 5. Cells were grown at 37°C on LB agarose and imaged

1244 automatically at 1 minute intervals for 60 minutes. Bar = 20 µm. Playback = 5 fps.

1245

1246 **Movie 2**. Time-lapse microscopy of Bas24 infection.

1247 Time-lapse microscopy comparing exponentially growing cells of *E. coli* MG1655Δ*araCBAD* in the

1248 absence (No system) and presence of GrwAB (+ GrwAB) production, after infection with Bas24 at MOI

1249 10. Cells were grown at 37°C on LB agarose + 5mM $CaCl_2$, 20mM $MgSO_4$, 0.2% arabinose and imaged

1250 automatically at 1 minute intervals for 180 minutes. Bar = 20 µm. Playback = 5 fps.

1251

1252 **Supplementary Figures**

1253 **Supplementary Fig. 1. Confidence metrics for AlphaFold3 models.**

1254 AlphaFold3 models of (**a**) WonAB and related systems (**b**) GrwAB, (**c**) *Vc*SduA and (**d**) DpdA are shown

1255 below predicted aligned error (PAE) plots and are coloured according to per residue predicted local

1256 distance difference test (pLDDT) score. The predicted template modelling (pTM) score, and where

1257 appropriate the interface predicted template modelling (ipTM) score, are shown below each model.